

Using empirical bode analysis, evaluating the delay margin of a fractional order-PI controller in a renewable-based distributed hybrid system

SOUMEN BISWAS¹, Provas Roy², and Kalyan chatterjee³

¹Dr BC Roy Engineering College

²Kalyani Government Engineering College

³Indian School of Mines

February 22, 2024

Abstract

In recent decades, renewable energy has emerged as one of the most promising alternatives to traditional energy sources for long-term, uninterrupted power supply. Engineers face numerous challenges when replacing renewable energy with conventional energy because the characteristics of solar and wind generation rapidly fluctuates with environmental conditions, resulting in large synchronizing imbalances between different units with system delays or communication delays in large electrical grids. They want to leverage computation delay margin to build a control mechanism that can handle a wide range of time delays (MADB). The authors of this article concentrate on the effects of the fractional integral order (FOI) on the stable parameter space for the regulation of a hybrid renewable energy based distributed system (DGS) in three-area AGC configuration. By altering the fractional order range, the delay margin (Δ) can be expanded, which can help to expand the stability region of a time delayed system. The stable parameter spaces of the controller are computed stability boundary based on the fractional integral order and time delay (Δ) values, and the present authors have developed asymptotic bode plot of time delayed Fractional-order proportional integral (FOPI) controller and computing delay margin (Δ) using gain margin (GM) and phase margin (PM) for this purpose. Honey badger algorithm (HBA) has been devised for fine-tuning the above-mentioned controller parameters. The controller's resilience is confirmed in the presence of random load perturbations, nonlinearities, and parameter fluctuation.

RESEARCH PAPER

Using empirical bode analysis, evaluating the delay margin of a fractional order-PI controller in a renewable-based distributed hybrid system

Soumen Biswas* | Provas Kumar Roy² | Kalyan Chatterjee³

¹Department of Electrical Engineering,
Indian Institute Of Technology, Dhanbad,
Jharkhand, India

²Department of Electrical Engineering,
Kalyani Government Engineering College,
Kalyani, West Bengal, India

³Department of Electrical Engineering,
Indian Institute Of Technology, Dhanbad,
Jharkhand, India

Correspondence

*Soumen Biswas. Email:
soumeniitkgp10@gmail.com

Present Address

Dr. B. C Roy Engineering College,
Durgapur, West Bengal, 713206, India

Summary

In recent decades, renewable energy has emerged as one of the most promising alternatives to traditional energy sources for long-term, uninterrupted power supply. Engineers face numerous challenges when replacing renewable energy with conventional energy because the characteristics of solar and wind generation rapidly fluctuates with environmental conditions, resulting in large synchronizing imbalances between different units with system delays or communication delays in large electrical grids. They want to leverage computation delay margin to build a control mechanism that can handle a wide range of time delays (MADB). The authors of this article concentrate on the effects of the fractional integral order (FOI) on the stable parameter space for the regulation of a hybrid renewable energy based distributed system (DGS) in three-area AGC configuration. By altering the fractional order range, the delay margin (τ_{dm}) can be expanded, which can help to expand the stability region of a time delayed system. The stable parameter spaces of the controller are computed stability boundary based on the fractional integral order and time delay (τ_d) values, and the present authors have developed asymptotic bode plot of time delayed Fractional-order proportional integral (FOPI) controller and computing delay margin (τ_{dm}) using gain margin (GM) and phase margin (PM) for this purpose. Honey badger algorithm (HBA) has been devised for fine-tuning the above-mentioned controller parameters. The controller's resilience is confirmed in the presence of random load perturbations, nonlinearities, and parameter fluctuation.

KEYWORDS:

Renewable based distributed hybrid system; Deregulation; FOPI controller; Time-Delay; Honey badger algorithm (HBA).

1 | INTRODUCTION

Renewable energy resources (RERs) have emerged as one of the most important sources for meeting ever-increasing load demand in the current world energy picture, owing to the rapid depletion of fossil fuel reserves (*i.e* coal and oil). As a result, for the past few decades, renewable resource research has been creating a road map for Green energy¹ across 143 countries in order to battle greenhouse effect, environmental pollution, and improve energy stability. The issues posed by global warming inspire

energy policymakers to continue their research in this field. Because of the rapid change in characteristics of diverse RERs such as solar² and wind into the current power system, some issues and constraints on the system's stability, security, operation, and control have become a major factor. With a big interconnected grid, this could result in a large synchronising imbalance between different units, as well as a large system latency or communication delay. As a result, researchers devote a large span of time and effort to identify control strategies to bring supply and demand into balance.

AGC ensures the overall system's reliability and power quality in the power sector. For the past few decades, an open communication channel³ has been allocated to inform exchange between the control unit and the generating station via a remote terminal unit. To run a deregulated market using open communication⁴ channels between GENCOs and DISCOs in different places, communication delay can be acceptable during the construction and operation of vast interconnected grids. However, in a vast area of interconnected grid, the impact of various non-linearities⁵ and communication delays has a significant impact on system instability. Along with that open networks expose numerous deficiencies in DGS-AGC services, such as increased communication lag, packet loss, and cyberattacks (e.g., false data injection), it's critical to figure out how communication variations in DGS-AGC affect system frequency stability in the future electric grid with the severe intensity. Depending on the exact communications networks, normal time delays—ranging from a few tens to hundreds of milliseconds are imposed when sending and processing remote signals. These delays are projected to increase when open communication channels and layered structures (DGS aggregators) are implemented, especially during periods of congested communication due to the massive amount of data interchange. The overall time delay also affects the AGC system's damping performance, resulting in undesirable results such as synchronism loss and system instability⁶. Within a wide area interconnected system, depending on the non-linearity, these delays could range from a few milliseconds to several hundreds of milliseconds⁷. As a result, determining the margin of allowable delay (MADB)⁸ is critical for understanding the consequences of delay-coupled systems.

According to a literature review, there are numerous methods for measuring the stability delay margin of a symmetrical system with time delay. These can be classified into two categories such as (i) delay margin analysis in frequency domain methods. (ii) delay margin analysis using time domain methods. In the frequency domain, the Shur-cohn approach⁹, Rackshius substitution¹⁰, Kronecker multiplication¹¹, root locus analysis¹² and empirical bode analysis.¹³ are the techniques for evaluating delay margins. Time delay evaluation in the time domain is demonstrated by the frequency sweeping test (FST)¹⁴ and the LMI¹⁵ approach. All of the existing approaches outlined above aim to compute delay margin only on the basis of stability, and to estimate delay margin values at which the LFC system will be marginally stable for a particular set of proportional-integral controller gains for various fractional orders. However, practical LFC systems cannot operate near such sites due to unacceptable frequency response oscillation. As a result, various design specifications such as gain margin (GM) and phase margin (PM) that provide a desired dynamic performance (*i.e.*, damping, overshoot, and settling time) must be taken into account in delay margin calculation in addition to the stability consideration.

The time domain direct technique fails to compute MADB when GM and PM are taken into account because it is not possible to incorporate GM & PM in the computational procedure. On the other side, frequency domain analysis may be able to solve this issue. By maximising an objective function, time-domain optimization algorithms look for the best controller settings. The control system that is developed can attain the best time-domain dynamic performance. However, system stability with gain and phase margin, as well as frequency-domain resilience performance should be assured at the same time.

On the other hand, a comprehensive literature study of many types of optimization techniques for tackling various types of issues has been conducted. Some traditional optimization techniques have strong convergence characteristics, but they suffer from a local optimality problem. Different heuristic strategies are efficiently adapted to various AGC problems to prevent this form of local optimality. For tuning integral-minus-tilt-derivative-control with filter (I-TDN), Babu *et al.* developed the hybrid crow-search with particle swarm optimization (hCA-PSO)¹⁶ technique. A novel adaptive distributed auction-based algorithm (ADAA)¹⁷ is employed for optimal mileage basis dispatch to quickly identify a high-quality dispatch scheme in a distributed way. Gravitational search optimization technique (GSA)¹⁸ is proposed for adjusting a dual proportional integral load frequency controller. Shouran *et al.*¹⁹ use the bees algorithm to the proportional integral derivative (PID)/ fuzzy PID filter (FPIDF)/Fractional-order PID (FOPID) controller to stabilize and balance the frequency in the multi source system at the rated value. In a multi-area system, Hakimuddin *et al.* employed the bacterial foraging optimization (BFA) technique²⁰ for the tuning of PID controller. To optimise the weighted matrices of the linear quadratic controller, Mohanty *et al.* proposed²¹ MFOA to a multi source system. Goswami *et al.* proposed a new heuristic algorithm called as the oppositional krill herd algorithm (OKHA)²² for solving multi-source AGC problems. For frequency control of multi-area power systems with wind power penetration, Elsis *et al.* proposed a novel Supervisor Fuzzy Nonlinear Sliding Mode Control²³. Biswas *et al.*²⁴ used the grasshopper

TABLE 1 The following is a taxonomy of the publications regarding the Time delay based AGC system that have been published.

Reference	AGC system						Area Type	Time delay	Controllers				Proto Type	(delay margin) τ_d Vs			Stability region with fraction order
	Thermal	Gas	Solar	hydro	Wind	EV			DGS*	I	PI	PID		FOPI	FACTs	I	
8	✓		✓		✓		Two	Yes		✓		✓			✓		
35	✓	✓		✓			Two	Yes			✓	✓	TID				
36	✓						single	Yes					MPC				
12	✓			✓			Two	Yes		✓					✓		
15	✓						Two	Yes		✓					✓		
5				✓			Single	Yes	✓						✓		
37				✓			Single	Yes	✓						✓		
1	✓		✓				Two	Yes			✓		PIDN				
2	✓						Two	Yes					MPC				
38	✓					✓	Two	Yes			✓		FPID				
39	✓						Two	Yes			✓		DMPID				
Present work	✓		✓		✓	✓	Three	Yes				✓				✓	✓

* Distributed generation system(DGS)

optimisation algorithm (GOA) to solve AGC in a deregulated environment. Hashim *et al.* recently developed honey badger algorithm (HBA)²⁵ for solving different kind of optimization problem.

However, literature survey on traditional controllers' prove that performance of controller has become worsen as nonlinearities increase and disturbance rejection capability decreases. Furthermore, the classical controller only takes countermeasures against disturbances when the control variable deviates from the reference level. The capacity to reject disturbances can be improved by incorporating fractional order into conventional controllers. To increase the performance of typical I/PI/PID²⁶ controllers, fractional order I (FOI)²⁷, Fractional-order PI (FOPI)²⁸, and FOPID²⁹ controllers are suggested. Some time fractional calculus theory (FCT) is applied to I/PI/PID controllers in FOI/FOPI/FOPID to improve their performance. Fractional-order (FO) controllers have been used to solve AGC problems in power systems during the last few years and have shown to be superior to traditional controllers. But some of the heuristic techniques have become very effective to enhance the performance of the fractional order controller such as ICA optimization³⁰ technique applied to CFFOPI–FOPID controller, FA optimised FOI/FOPI/2DOF-FOPID³¹ controllers to single- and two-area power systems. Nayak *et al.*³² suggested a hybrid SSA–SA based three-degree-of-freedom fractional-order PID controller on two-area hybrid system. A Non-fragile PID³³ is also used to regulate the frequency of an interconnected multi-source (restructured environment) system.

This paper addresses an RERs-based hybrid system with constant time delay due to the presence of different non linearities in the system. The main goal of this paper is to develop a relationship between delay margin (τ_{dm}) and fractional order (λ) in the K_p – K_I parameter plane, which is not only robustly stabilise a uncertain control systems with varying rate $\mu = 0$, but also specifically determine the stability region for different order (λ) of FOPI controller. This is performed by using empirical bode analysis to determine delay margin³⁴ using GM and PM for various fractional orders of FOPI (λ varying from 0 to 1) controllers.

1.1 | Novel objective of the current research work:-

1. This article proposes a method for designing delay dependent stable systems using empirical bode analysis (EBA) and delay margin calculation (MADB) of constant time delay systems.
2. This study also demonstrates how non-linearities can generate delays, lowering the dynamic performance of an AGC system and, in the worst-case scenario, causing a significant instability concern. The delay margin for a fractional order PI (FOPI) controller is estimated using the proposed (EBA)³⁴ method, and the controller is designed using a systematic methodology.
3. To test the efficacy of the suggested³³ approach on a three-area renewable based³³ hybrid system with distributed generation⁴⁰ in a deregulated environment, for constant delays are considered ($\mu = 0$).
4. The simulation results validate the accuracy of the empirical bode analysis used to calculate the delay margin of the FOPI controller for a certain fractional order range ($\lambda = 0$ to 1). Fractional order increases (λ) may enhance delay margin

(τ_{dm}) for a specific control parameter set (K_P & K_I) and vice versa. As a result, greater order fraction (λ) is preferable to smaller fractional orders, which are used to optimize the hybrid system's dynamic response with a set delay margin. HBA algorithm²⁵ has been devised for fine-tuning of the above control parameters.

2 | DESCRIPTION OF THE PROPOSED SYSTEM:-

A two-area thermal²¹ system has been used as the primary test system (Test system-1) in this paper. Initially, test system-1 was used to test the efficacy of the HBA algorithm against other evolutionary algorithms such as BFA²⁰, MFOA²¹, OKHA²², and GOA²⁴ and a comparative study was performed²⁵. Afterward, the research is extended to a three-area hybrid system with distributed generation in a deregulated environment (test system-2)²⁴ that includes non-conventional resources such as solar and wind power plants with distributed generation⁴⁰. For test system-1, the total power rating of the power system is 600 MW, with each area consists of 300 MW units. Total output power for test system-2 has been set at 1600 MW, with 750 MW, 50 MW, 600 MW, and 200 MW are allocated to thermal, wind, solar, and distributed generation, respectively, as illustrated in Fig. 1. The details of distributed generation given below:-

2.1 | Distributed generation system(DGS):-

• Wind turbine generator (WTG):-

Wind power, also known as wind energy, is the use of air movement through wind turbines that fluctuates with time and is connected to previous wind speeds. The auto regressive and moving average time-series models can be used to represent the changes of wind speed over time. Mathematical equation of wind speed can be expressed as:-

$$y(t) = \sum_{i=1}^n \Phi_i y_{t-i} + \alpha_t - \sum_{j=1}^m \theta_j \alpha_{t-j} \quad (1)$$

where Φ_i , α_t and θ_j are auto regressive parameter, moving average parameter, and a normal white noise process with zero mean in order. Calculation for the speed of wind can be calculated by (2).

$$\omega_{WT} = \eta_{WT} + \sigma_{WT}x(t) \quad (2)$$

where the mean and standard deviation of wind speed are μ_{WT} and σ_{WT} , respectively. The output power of wind power generation is calculated using (3) which is shown in Fig. 2.

$$\begin{aligned} P_{WTG} &= 0; \omega_{WT} < W_{in}, \omega_{WT} > W_{out} \\ P_{WTG} &= \lambda (WS - W_{in}); W_{in} < \omega_{WT} < W_{rs} \\ P_{WTG} &= 1; W_{rs} < \omega_{WT} < W_{out} \end{aligned} \quad (3)$$

Equation (3) represents cut-in, rated, and cut-out wind speed, respectively, where the straight line passes through the points of cut-in and rated wind speed. The linear approximated model of wind turbine generator for LFC analysis is given by the following first-order time-lag transfer function:-

$$G_{WTG}(s) = \frac{K_{WTG}}{(1+sT_{WTG})} \quad (4)$$

where ΔP_{WTG} represents change in power output in wind power generator.

• Aqua Electrolyzer & Fuel Cell:-

Hydrogen cell is the alternative resources for electric power generation. Aqual electrolyzer take a portion of $(1 - \gamma)$ wind turbine generator, which can be used to disintegrate water molecules into hydrogen gas, which can then be utilised to generate electricity via a fuel cell. AE & FC play an important role to produce electrical power in distributed generation system. Transfer function of AE & FC are defined by:-

$$\begin{aligned} G_{AE} &= \frac{K_{AE}}{1+sT_{AE}} \\ G_{FC} &= \frac{K_{FC}}{1+sT_{FC}} \end{aligned} \quad (5)$$

Gain of AE & FC are given by K_{AE} & K_{FC} . And T_{AE} & T_{FC} are the time constant of AE & FC.

• Diesel unit

Usually a diesel power station (also known as stand-by power station) uses a diesel engine as prime mover for the generation of electrical energy. This power station is working as auxiliary power generating units which can be located where it is actually

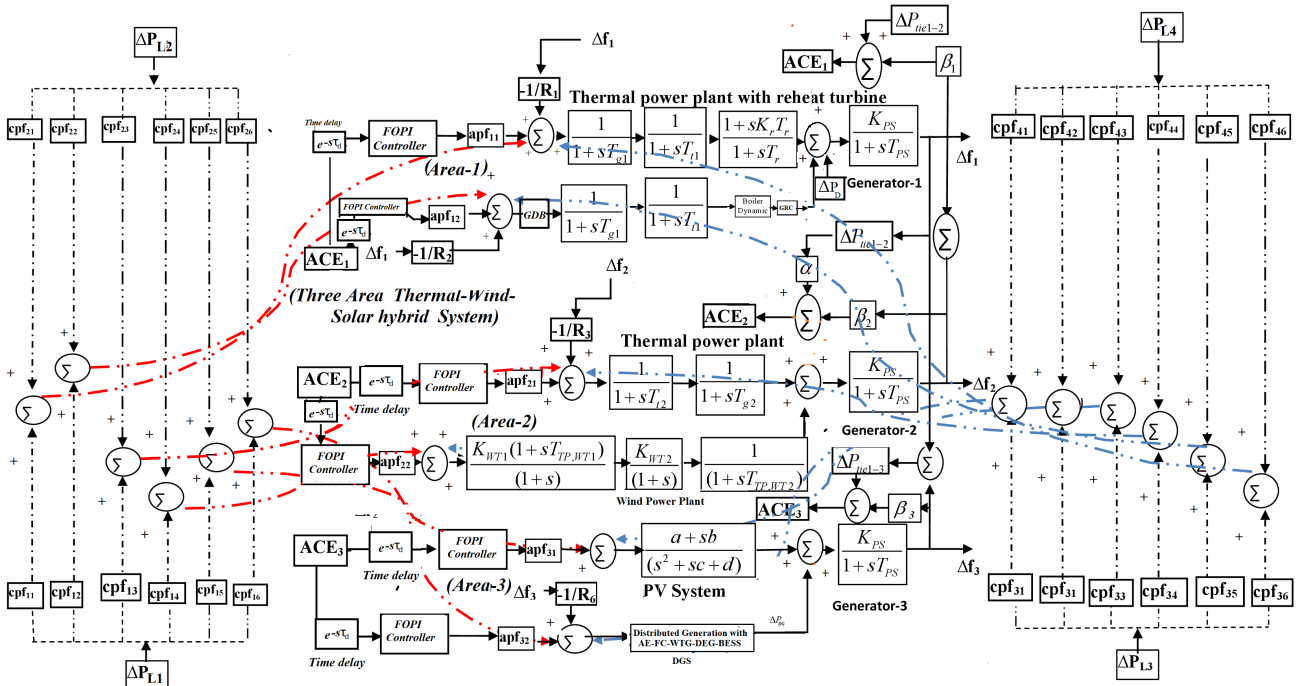


FIGURE 1 Linearized model of three-area renewable based (Solar-PV) system with distributed generation

required. This kind of power station can be used to produce limited amounts of electrical energy which can be used as emergency supply stations. The transfer function of Diesel power plant is stated in (6).

$$\frac{K_{DEPG}}{1 + sT_{DEPG}} \quad (6)$$

where ΔP_{DEPG} is incremental change of output power from diesel power plant; K_{DEPG} and T_{DEPG} are the gain and time constant of diesel unit plant.

• Battery renewable energy sources (BESS)

Storage renewable energy resources are used to maintain the constant power flow through tie-line during intermittent load demand, specially in the peak demand period. The role of battery energy storage devices (such as Tesla power wall battery, redox-flow battery, super-magnetic energy storage devices) in the grid are elucidated below:-

1. Maintain the proper coordination between different generating units.
2. Optimize the operating cost.
3. The BESS consists of power converter with bank of D.C batteries. Power converter is helpful for bi-directional power conversion (DC to AC and Vice Versa) as per the grid requirement.
4. It is also used to neutralize the system harmonics and control the system voltage.
5. The transfer function of Battery energy storage system stated as:-

$$\frac{K_{BESS}}{1 + sT_{BESS}} \quad (7)$$

where K_{BESS} & T_{BESS} are the gain value and time constant of battery energy storage system.

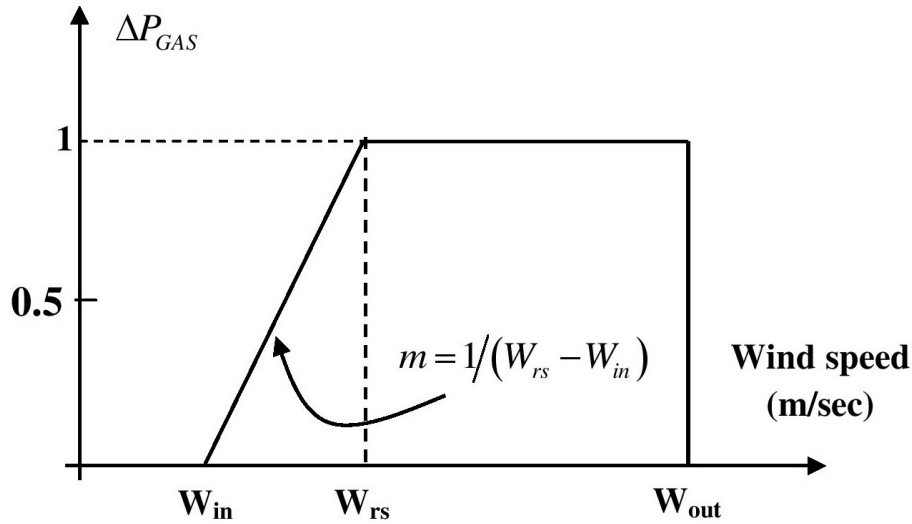


FIGURE 2 Characteristic of wind turbine

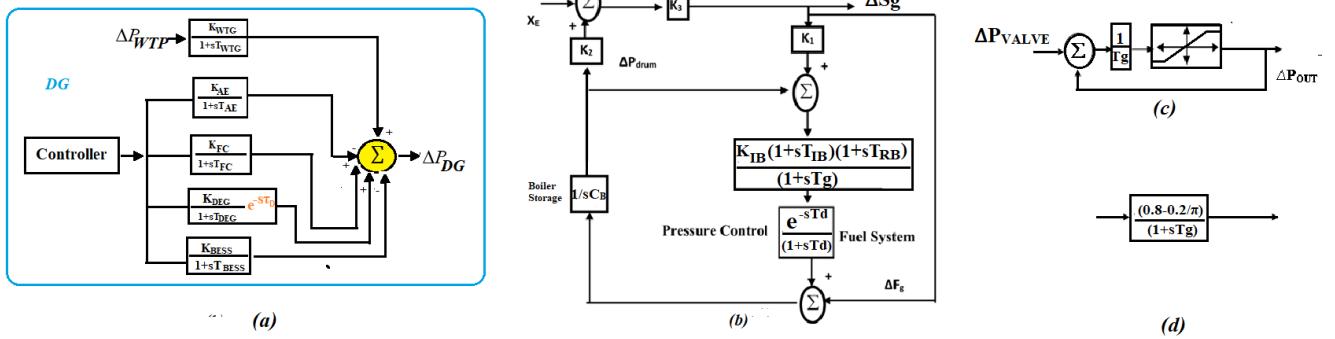


FIGURE 3 (a) Linearized model of distributed system(DGS).(b) Schematic block diagram of boiler dynamics in test system-2. (c) Schematic Block diagram of GRC in test system-2.(d) schematic diagram of governor dead-band in test system 2.

As shown in Figs. 3(b-d), some non-linearities are included to the thermal unit, such as GDB (Governor Dead-band), BD (Boiler Dynamics), and GRC (Governor rate constraints), to test the effectiveness of the HBA algorithm in a realistic environment. GRC has been calculated to be 3% every minute in this literature. Back-slash non-linearity of 2% for thermal system and 0.05 % for hydro system are usually considered. In a deregulated environment, this research studies a delay-dependent stability. Before the controller, a single delay is taken into account, which is caused by non-linearities and a lack of synchronism among solar-wind-thermal power plants. It is expressed by an exponential term, $e^{-s\tau_d}$ ^{36,41} where τ_d indicates the total time delay in the system that has been considered.

The use of a three-area hybrid system (thermal, wind, and solar)with distributed generation system is being studied²⁴ under the deregulated environment. As previously stated, the total study was conducted in a deregulated environment, with the power contracts between various DISCOs (Distribution companies) and GENCOS (Generation companies) are reflected in the distribution participation matrix (DPM) for the various scenarios (unilateral, bi-lateral and contract-violation).

Hence, DPM can be defined as:-

$$\text{DPM} = \begin{bmatrix} cpf_{11} & cpf_{12} & cpf_{13} & cpf_{14} \\ cpf_{21} & cpf_{22} & cpf_{23} & cpf_{24} \\ cpf_{31} & cpf_{32} & cpf_{33} & cpf_{34} \\ cpf_{41} & cpf_{42} & cpf_{43} & cpf_{44} \\ cpf_{51} & cpf_{52} & cpf_{53} & cpf_{54} \\ cpf_{61} & cpf_{62} & cpf_{63} & cpf_{64} \end{bmatrix} \quad (8)$$

The sum of all entities in a DPM matrix placed in a column should be equal to one as represented below :-

$$\sum_{i=1}^{\text{NGENCO}} CP_{ij} = 1; \text{for } j = 1, 2, 3, \dots, \dots \{NDISCO\}, (NDISCO = 4) \quad (9)$$

3 | GENERALIZED FORM OF TRANSFER FUNCTION OF A FRACTIONAL ORDER TIME DELAYED SYSTEM :-

The transfer function of a fractional order system is given by:-

$$G_{FO}(s^\gamma) = \frac{a_n s^{\gamma n} + a_{n-1} s^{\gamma(n-1)} + \dots + a_0 s^{\gamma 0}}{C_m s^{\gamma m} + C_{m-1} s^{\gamma(m-1)} + \dots + C_0 s^{\gamma 0}} = \frac{\Delta_N(s^\gamma)}{\Delta_D(s^\gamma)} \quad (10)$$

The transfer function of fractional order system is given in (10). Here, transfer function exists a common division $Q \in S$ such that $\gamma_i = pf_i (i = 0, 1, \dots, m)$, $\alpha_k = pf_k (k = 0, 1, 2, \dots, n)$; e_i , where P is called the commensurate order, which can be rotational or irrational. Therefore, the transfer function can be represented as:-

$$\tau(s) = \frac{y(s)}{u(s)} = \frac{M(s^P)}{N(s^P)} = \frac{M(q)}{N(q)} \quad (11)$$

Where $q = s^\gamma$ in the polynomial equation. The generalized form of fractional order system is given by:-

$$G_{FO}(q) = \frac{\prod_{k=0}^{n_1} (q + d_k) \prod_{i=0}^{n_2} (c_i q^2 + e_k^q + f_i)}{\prod_{j=0}^{n_3} (q + g_j) \prod_{m=0}^{n_4} (h_m q^2 + o_m q + z_m)} \quad (12)$$

Where $d_k (k = 0, 1, 2, \dots, n_1)$, c_i , e_k , $f_i (i = 0, 1, \dots, n_2)$, $g_j (j = 0, 1, 2, 3, \dots, n_3)$, h_m , o_m , $z_m (m = 0, 1, \dots, n_4)$ are positive integers. Now substituting $q = s^p$, (12) can be rewritten as:-

$$G_{FO}(s^\gamma) = \frac{\prod_{k=0}^{n_1} (s^p + d_k) \prod_{i=0}^{n_2} (c_i q^2 + e_k^q + f_i)}{\prod_{j=0}^{n_3} (s^p + g_j) \prod_{m=0}^{n_4} (h_m q^2 + o_m q + z_m)} = \frac{\Delta_N(s^\gamma)}{\Delta_D(s^\gamma)} \quad (13)$$

This method also applicable for analyzing the fractional order non-linear time delayed system. Let us consider transfer function of a fractional order linear time delayed system:-

$$G_{FO}(s^\lambda) = \frac{\Delta_{N0}(s^\lambda) + \sum_{j=1}^{p_1} \Delta_{Nj}(s^\lambda) e^{-\tau_j s}}{\Delta_{D0}(s^\lambda) + \sum_{i=1}^{p_2} \Delta_{Di}(s^\lambda) e^{-\tau_i s}} = \frac{\Delta_N(s^\lambda)}{\Delta_D(s^\lambda)} \quad (14)$$

Where, τ_d is the delay time, and real coefficients of fractional order polynomial are given by:-

$$\Delta_{Di}(s^\lambda) = \sum_{k=1}^m q_{jk} s^{\lambda_{DK}} \dots i \in 0, 1, 2, \dots, p_1$$

and

$$\Delta_{Nj}(s^\lambda) = \sum_{k=1}^n z_{jk} s^{\lambda_{NK}} \dots j = 0, 1, 2, \dots, p_2 \quad (15)$$

When λ_{DK} & λ_{NK} are the non-real native numbers.

The transfer function of fractional order system is commensurate order if and only if λ_{DK} and $\lambda_{DK} \in k\lambda (k = 0, 1, \dots, n)$ and $\lambda_{NK} \in k\alpha (k = 0, 1, 2, 3, \dots, n)$ otherwise it is in the range of non-commensurate order. Now the characteristics

equation of a commensurate order fractional order system is given by:-

$$\Delta D(s^\lambda) = \Delta_D(s^\lambda) + \sum_{i=1}^{y_1} \Delta_{D_i}(s^\lambda) e^{-\tau_i s} \quad (16)$$

3.1 | Evaluation of delay margin using Empirical bode analysis (EBA) of time delayed fractional controller

A study of fractional order system proves that the equation carries fractional pole and zeros in form of double term. Hence, it is helpful to construct asymptotic bode plots $G(s)$ by adding or subtracting FO system which is similar to that PI^λ .

In this article, authors have used gain plot and phase plot to analyze the stability of a time delayed fractional order controller, which can be defined as:-

$$G_{FOC}(s^\lambda) = G_c(s^\lambda) = \frac{\Delta_{Nc}(s^\lambda)}{\Delta_{Dc}(s^\lambda)} = \frac{\Delta_{Nc}(s^\lambda)\Delta_{Dc}^*(s^\lambda)}{\Delta_{Dc}^*(s^\lambda)\Delta_{Dc}(s^\lambda)} = \frac{\Delta_{Nc}(s^\lambda)\Delta_{Dc}^*(s^\lambda)}{|\Delta_{Dc}(s^\lambda)|^2} \quad (17)$$

Equate the imaginary portion of the numerator equal to zero to get the value of phase crossover frequency:

$$im[\Delta_{Nc}(j\omega_{pc})^\lambda \Delta_{Dc}^*(j\omega_{pc})] = 0; \quad \{putting s = j\omega = j\omega_{pc}\} \quad (18)$$

Gain margin using phase crossover frequency (ω_{pc}) is obtained from (18).

$$GM = -1/G_c(j\omega_{pc})^\lambda \quad (19)$$

Obtain the value of gain crossover frequency (ω_{gc}) using following equation:-

$$|G_c(j\omega_{gc})^\lambda|^2 = 1 = |\Delta_{Nc}(j\omega_{gc})^\lambda|^2 = |\Delta_{Dc}(j\omega_{gc})^\lambda|^2 \quad (20)$$

Value of phase margin using gain crossover frequency is given by:-

$$PM = 180^0 + \angle G(j\omega_{gc})^\lambda \quad (21)$$

Consider time delay effect into the fractional order controller:-

$$G_{FOC}(s^\lambda) = G_c e^{-s\tau_d} \quad (22)$$

Where τ_d =Time delay.

Condition for fractional order controller in the verge of stability is given by:-

$$G_c(s^\lambda) e^{-j\omega_{gc}\tau_{dm}} = -1 \quad (23)$$

Where τ_{dm} =value of delay margin.

Now satisfying (23) for stability, modified equation can be rewritten as:-

$$\angle G_c(j\omega_{gc})^\lambda - (\omega_{gc})^\lambda \tau_{dm} \times \frac{180^0}{\pi} = -180^0 \quad (24)$$

Evaluation of delay margin using (24) is given by.

$$\tau_{dm} = \frac{PM}{(\omega_{gc})^\lambda} \times \frac{\pi}{180^0} = \frac{180^0 + \angle G(j\omega_{gc})^\lambda}{(\omega_{gc})^\lambda} \times \frac{\pi}{180^0} \quad (25)$$

4 | THE PROPOSED SYSTEM'S MATHEMATIC FORMULATION :-

The delay-margin is calculated by the authors of this research in order to achieve generation-load balance at their schedule level, in order to analyse the suggested hybrid system's delay-dependent stability. The choice of objective function has a significant impact on the dynamic response of the system.

4.1 | Objective function

The performance index is determined by using a defined objective function to obtain optimum controller gain. Control error is responsible for delivering control signals for the FOPI controller for different fractional orders (λ) for constant ($\mu = 0.0$) time delay system. Objective function (J) is defined as the linear combination of frequency deviation and tie-line power. Integral squared error (ISE) technique is commonly used in controller design. The construction of an optimization based controller necessitates the selection of acceptable weighted values of frequency deviation for both areas in the performance indices (J) based on the intended requirements and constraints. Large control signals were generated by weighting solely frequency and tie-line power deviations in the performance index, which quickly forces frequency and tie-line deviations to zero. The objective function treated as performance index is given by:-

$$j = \int_0^{t_{\min}} (\Delta P_{tie1-2}^2 + \alpha \Delta f_1^2 + \delta \Delta f_2^2) dt \quad (26)$$

The values of α and δ are assumed to be equal in this situation, *i.e.* 0.056. The weighted values for the frequency deviation in both locations, α and δ , are used to assign equal importance to tie-line power and frequency responses. Aside from that, the authors have presented a new Honey badger technique to improve the FOPI controller's K_P & K_I . Section 5.2.2 outlines the steps for optimising the gain value of a FOPI controller with various fractional orders.

4.2 | System constraints

The suggested AGC system can be thought of as a restricted optimization problem with the following constraints:-

$$\begin{aligned} K_{P1,\min} &\leq K_{P1} \leq K_{P1,\max}; K_{I1,\min} \leq K_{I1} \leq K_{I1,\max}; \\ K_{P2,\min} &\leq K_{P2} \leq K_{P2,\max}; K_{I2,\min} \leq K_{I2} \leq K_{I2,\max}; \\ K_{P3,\min} &\leq K_{P3} \leq K_{P3,\max}; K_{I3,\min} \leq K_{I3} \leq K_{I3,\max}; \\ \lambda_{\min} &\leq \lambda \leq \lambda_{\max}; \end{aligned} \quad (27)$$

where the control parameters for case-1 (K_P , K_I) are in the range of 0 to 2. Only the performance of the *FOPI* controller with fractional order (λ) has been examined for different ranges of delay in case-2 to estimate the delay margin (using empirical bode analysis). Where the gain value of K_P & K_I fractional order (λ) of *FOPI* controllers is set between 0.1 and 0.8.

4.3 | Mathematical explanation of MADB calculation for time delayed fractional-order PI controller

In this article, optimal design of PI controller is determined with the transfer function expressed in (28).

$$T_{FO-PI} = G_c(s) = \left(K_P + \frac{K_I}{s^\lambda} \right) = K_P + K_I \omega^\lambda \cos(\pi\lambda/2) - j k_i \omega^{-\lambda} \sin(\pi\lambda/2) \quad (28)$$

The stability margin of time delay is established by evaluating delay margin of fractional-order PI controller. For this purpose, we substitute $s = j\omega$ in the time delayed FOPI controller to evaluate the characteristic equation :-

$$T_{FO-PI} = G_c(j\omega) = \left(K_P + \frac{K_I}{j\omega^\lambda} \right) e^{-j\omega\tau_d} = K_P + K_I \omega^\lambda \cos(\pi\lambda/2) - j k_i \omega^{-\lambda} \sin(\pi\lambda/2) e^{-j(\arctan(\pi\lambda/2))} \quad (29)$$

Here, ω_{gc} & ω_{pc} are the gain crossover frequency and phase crossover frequency of the FOPI controller.

The necessary and sufficient condition to meet the controller's robustness requirement is stated by:-

(i) Phase margin (P.M) at gain crossover frequency (G.C.F) :-

$$\angle G(j\omega_{gc}) = PM - \pi \quad (30)$$

(ii) Gain of the system at G.C.F:-

$$\left| G(j\omega_{gc}) \right| = 1 \quad (31)$$

(iii) Phase at phase crossover over frequency (P.C.F):-

$$\angle G(j\omega_{pc}) = -\pi \quad (32)$$

(iv) Gain of the system at phase crossover frequency is given by:-

$$\left|G(j\omega_{pc})\right| = 10^{GM/20} \quad (33)$$

Applying (30 & (31) in (29), Gain value & Phase value of FOPI controller can be obtained using:-

$$|C(j\omega)| = \sqrt{K_p + K_i\omega^\lambda \cos(\pi\lambda/2)^2 + (-K_i\omega^{-\lambda} \sin(\pi\lambda/2))^2} = 1 \quad (34)$$

and

$$\angle C(j\omega) = \arctan \left[\frac{-K_i \sin(\pi\lambda/2)}{K_p + K_i\omega^{-\lambda} \cos(\pi\lambda/2)} \right] = PM - \pi \quad (35)$$

The following equation can be used to find a fractional order PI controller that ensures the desired gain crossover frequency:-

$$K_p = \pm \frac{10^{GM/20} \cot(\pi\lambda/2) \tan(\phi_2)}{\sqrt{1 + (\tan \phi_2)^2}} \quad (36)$$

and

$$K_i = \pm \frac{10^{GM/20} \cos(\pi\lambda/2) \tan(\phi_2)}{\sqrt{1 + (\tan \phi_2)^2}} \quad \text{Where } \phi_2 = -\pi \tan \arccot(\tau\omega_{pc}) \quad (37)$$

The value of K_p & K_i has been utilize to define basic fractional order controller and simulate individual asymptotic magnitude of bode plot. Moreover, the stability condition is judge through evaluating delay margin (τ_{dm}) for different fractional order controller ($\lambda = 0.2, 0.4, \&, 0.8$). The value of delay margin (τ_{dm}) is evaluated using eqn.(36) and eqn.(37) are given in Tables 3-6.

4.3.1 | Algorithm steps for computation of MADB

The proposed approach for MADB computation using gain margin & phase margin includes the following steps:-

- Step 1: Without a controller, create a linearized model of a hybrid system (Solar-wind-thermal with DGS).
- Step 2: The state space equation of the AGC system with the $P - I$ controller is established. Afterword, the linearized hybrid system with time varying delay is used to design the controller.
- Step 3: Based on the linearized model obtained in step 2, the delay margin is calculated. After evaluating gain margin (GM) and phase margin (PM), the value K_p & K_i using the HBA algorithm is obtained, and system stability is analyzed by satisfying (24) & (25).
- Step 4: The search interval for calculating delay margin starts with τ_i and concludes with τ_f . Furthermore, the following steps are used to determine a specified time delay τ_d for a collection of K_p & K_i :-
1. Get transfer function of Fractional order P-I controller for different time delay τ_i and ends with τ_f .
 2. Evaluating gain margin and phase margin for different time delayed FOPI-controllers.
 3. Calculate delay margin using (24) & (25)
 4. Continue the searching process $\tau_{int} = \left| \tau_i - \tau_f \right|$ with τ_d , and if $\tau_{int} \geq \tau_d$, go to step 1 for further tuning. The output is treated as delay margin of τ_d .
- Step 5: The stability of the abovementioned hybrid system is then verified using a simulation approach with a particular time delay τ_d for $\tau_d \leq \tau_{set}$.

5 | PROPOSED HONEY BRADGER ALGORITHM (HBA)

5.1 | Honey bradger algorithm

Honey bradger (HBA) algorithm is based on the behaviour of a mammal fluffly found in rain forest of asia-pacific and indian sub-continent and it is well known for its fearless nature. Throughout the world sixty different species of fearless forager preys exists, out of which 12 are recognized as honey bradger subspecies exists in Asia Pacific region. HBA algorithm is designed using the

foraging behaviour of honey bradger. Searching for food source, honey bradger either digs and smell or follows honey-bird. They complete their tasks in two different modes such as digging mode and honey mode. In first step, its uses its smelling ability to select the appropriate location for digging and in 2nd phase, honey bradger takes the help of honey guide bird to directly locate beehive.

5.2 | Mathematical model

As discussed in the previous section, HBA is classified into two different phases. They are (i) digging phase (ii) honey phase.

In this part, authors have explained the mathematical model of HBA algorithm. Exploration and exploitation capability of the algorithm help it to get the optimal solution of a global optimization problem. At initial phase, population of n number of solution with $D - dimension$ is represented as:-

$$\begin{bmatrix} \varphi_{11} & \varphi_{12} & \varphi_{13} & \cdots & \varphi_{1D} \\ \varphi_{21} & \varphi_{22} & \varphi_{23} & \cdots & \varphi_{2D} \\ \varphi_{31} & \varphi_{32} & \varphi_{33} & \cdots & \varphi_{3D} \\ \vdots & \vdots & \vdots & \cdots & \vdots \\ \vdots & \vdots & \vdots & \cdots & \vdots \\ \varphi_{n1} & \varphi_{n2} & \varphi_{n3} & \cdots & \varphi_{nD} \end{bmatrix} \quad (38)$$

Where, set of badget up to i^{th} position is given by:- $\varphi_i = [\varphi_i^1, \varphi_i^2, \varphi_i^3, \dots, \varphi_i^n]$.

5.2.1 | Steps of optimization technique

Step 1: Initialization:-

Initialize the number of honey bradger with particular size N is given by:-

$$\varphi_k = lb_k \times rb_k (ub_k - lb_k) \text{ where } r_k \text{ lies in between } 0 \text{ to } 1. \quad (39)$$

Here, φ_k is the honey bradger at K^{th} position to a candidate solution of honey bradger with population size N ; ub_k & lb_k are the lower bound and upper bound in the search domain.

Step 2: Defining intensity:-

The small I_i intensity of the prey is inversely proportional to honey bradger and is given by following equation:-

$$I_i = r_2 \times \frac{s}{4\pi d_i^2} \quad (40)$$

where r_2 is random variable lies between 0 to 1; $s = (\varphi_i - \varphi_{i+1})^2$ & $d_i = x_{prey} - x_i$.

Step 3: Density Factor:- Density factor (β) is continuous time varying randomization used for constant transformation from exploration to exploitation. Update new position with decreasing factor β which can be randomized with time, using (43).

$$\beta = C \times \exp\left(\frac{-\tau}{\tau_{\max}}\right) \quad (41)$$

Where $C \geq 1$; τ_{\max} = maximum iteration time.

Step 4: Escaping local optima:- This step, along with the two next ones, is used to get through local optima areas. In this context, the proposed approach employs a flag F that changes the search direction, allowing agents to thoroughly investigate the search space.

Step 5: Updating the agent position:-

As previously stated, the HBA position update process (φ_{new}) is split into two phases: "digging phase" and "honey phase".

1. Digging phase:-

In the digging phase, a honey bradger performs action similar to cardioid shape which can be written as:-

$$\varphi_{new} = \varphi_{prey} + F \times \gamma \times I \times \varphi_{prey} + F \times r_3 \times \beta \times d_i \times \geq |\cos(2\pi r_4) \times [1 - \cos(2\pi r_3)]| \quad (42)$$

Where φ_{prey} is position of the prey which is the best position found so far; $r_3, r_4, & r_5$ are the three different random numbers lies between 0 to 1; F works as a flag that alters the search direction by the following equation:-

$$F = \begin{cases} 1 & \text{if } r_6 \leq 5, r_6 \text{ is the random number.} \\ -1 & \text{else lies between 0 to 1.} \end{cases} \quad (43)$$

2. Honey phase:-

In this case where a honey bradger follows honey guide bird to find the food source, can be written by following equation:-

$$\varphi_{new} = \varphi_{prey} + F \times r_1 \times \beta \times d_1 \quad (44)$$

Where r_1 lies in between 0 to 1; φ_{new} is refer to the new position of honey bradger; φ_{prey} refers to the new position of honey bradger; Value of β & F are determined using (41) & (43), respectively.

5.2.2 | Pseudo-code for implementing the HBA algorithm into a time-delayed hybrid system:-

```

Set parameters  $\tau_{max}, N, \gamma$  &  $C$ 
Initialize the parameters with arbitrary position. Evaluate the fitness value of each honey bridge  $\varphi_i$ 
(i,1,2.....N).
Save best position  $\varphi_{prey}$  to calculate fitness value  $f_{prey}$ .
while  $t \leq \tau_{max,do}$  do
  for  $m = 1 : N$  do
    Calculate the intensity  $I_i$ , using (40)
    if  $r < 0.5$  then
      Update the position  $\varphi_{new}$  using (42)
    else
      Update the new position  $\varphi_{new}$  using (44)
    end if
    Evaluate  $\varphi_{new}$  to evaluate  $f_{new}$ 
    if  $f_{new} \leq f_i$  then
      Set  $\varphi_i = \varphi_{new}$  and  $f_i = f_{new}$ 
    end if
    if  $f_{new} \leq f_i$  then
       $\varphi_{prey} = \varphi_{new}$  &  $f_{prey} = f_{new}$ 
    end if
  end for
   $t = t + 1$ 
end while

```

5.2.3 | Application of the HBA algorithm to a time-delayed AGC problem:-

- Step 1: Using (39), initialise the control variables $K_{p1}, K_{I1}, K_{p2}, K_{I2}, K_{p3}, K_{I3}$ & λ . Calculate the appropriate control variables' fitness value at the m^{th} position. Here, T is the maximum number of iterations, and N is the population size.
- Step 2: The maximum & minimum operating limits are used to standardise the value of control parameters.
- Step 3: Depending on the population size, several sets of control variables are formed to generate matrix pools.
- Step 4: Equation (44) is used to update the control variables.
- Step 5: For each new updated control variable position, calculate the objective function j until an optimal solution is discovered.

6 | SIMULATION RESULTS:-

The suggested HBA, MFOA, BFA, OKHA and GOA algorithms are coded in m. files, and the AGC system is designed using MATLAB/SIMULINK tools. The total number of iterations for HBA, MFOA, OKHA & GOA approaches for tuning control

TABLE 2 Gain values PID controllers of two-area system

PID controller	K_{p1}	K_{i1}	K_{d1}	K_{p2}	K_{i2}	K_{d2}	$(OBJ \times 10^{-5})$	Δf_1			Δf_2			ΔP_{tie1-2}		
								$OS \times 10^{-6}$	$US \times 10^{-4}$	SS	$OS \times 10^{-6}$	$US \times 10^{-4}$	SS	$OS \times 10^{-6}$	$US \times 10^{-4}$	SS
GA ²¹	0.939	0.7998	0.5636	0.52	0.4775	0.705	1.244	2.576	-73.40	9.23	0	-11.03	11.4	0	-134.2	23.1
BFA ²⁰	1.4964	0.9973	0.9903	1.39	0.8324	0.925	0.792	2.059	-54.3	8.05	0	-6.912	10.3	0	-107.5	23.3
OKHA ²²	1.6723	0.8694	1.2345	1.01	0.6542	1.167	0.259	1.0254	-48.24	6.25	0	-6.02	7.95	0	-69.25	12.3
GOA ²⁴	1.3965	1.294	0.9673	0.67	1.2915	0.1.0123	0.055	0.946	-42	3.05	0	-4.82	4.62	0	-64.38	10.3
HBA	1.46	0.67	0.97	1.15	0.9792	1.0272	0.016	0.401	-0.4	2.25	0	-2.12	3.06	0	-41.24	7.9

parameters are considered as 150 in both cases. Furthermore, empirical bode analysis is utilised to examine the delay margin of stability for various delay ranges. To control the mutation in the perturbation process, the controllers are set to a range of 0 to 6 for test system-1 and 0.1 to 0.8 for test system-2, and the simulation is run in MATLAB (R2014a) on an Intel Core I3 CPU running at 2.20 GHz. To assess the success of the suggested approach, a variety of simulation combinations are used to fine-tune the HBA adjusted control parameters.

6.1 | Case study with two-area thermal-system:-

Firstly, the efficacy of the suggested HBA method is evaluated through dynamic responses of two-area thermal system²¹. Appendix 1 lists the values of system parameters for a two-area thermal unit. Table 2 shows how to maximize the gain value of the PID controller and the objective function 'J' with a 20% step load disturbance at area-1 using various strategies. When proposed method is compared to other methods, the objective function 'J' and other response characteristics such as overshoot, undershoot, and steady state error are found to be smaller with the HBA methodology. The second best value of the objective function comes from a GOA tuned²⁴ PID. Figs. 4(a-c) shows that the HBA²⁵ optimised PID controller gives best outcomes than other heuristic techniques like OKHA, BFA, and MFOA in terms of dynamic responses. The dynamic responses of Δf_1 , Δf_2 , and ΔP_{tie1-2} are improved with the suggested HBA optimised PID controllers, as shown in Table 2. When the suggested HBA optimised PID is compared with GOA, OKHA²², and BFA²⁰ optimised PID, objective function (ISE) is improved by 38.81%, 67.72 %, and 78.2%, respectively. HBA optimised controllers improves the dynamic response of ' Δf_1 ' i.e. overshoot and undershoot by 12.7 %, 22.3 %, 51.2 %, 20.08 %, 67.2 %, and 95 %, respectively, as compared to OKHA²², BFA, and GA tuned PID controllers. By optimising the PID controller using additional techniques such as OKHA, BFA, and MFOA²¹, the efficacy of the suggested HBA algorithm may be explored.

6.2 | Case study with time delays using FOPI controller:-

6.2.1 | A deregulated environment with a renewable multi-source system:

The authors have conducted an experiment using a time-delayed AGC model of a three-area renewable-based hybrid system with distributed generation in this research. Appendix-B depicts the hybrid system's parameter values. The gain and phase margins³⁴ for the provided AGC system outlined in section 3 are used to calculate the Margin for Allowable Delay (MADB). For constant time delay with varying rate $\mu = 0.0$, delay margins of τ_d for different values of K_p & K_I for different fractional order (λ) are obtained, which can aid in the design of FOPI controllers for a wide range of stable operation of the proposed three-area hybrid system.

Here, a renewable hybrid system with a FOPI controller is studied in deregulated context. Tables 3-6 show the delay margin of τ_d determined using empirical bode analysis for different value of λ in K_p & K_I plane. The delay margin is evaluated for different set of fractional order through proposed technique to identify the stability region of the proposed time delayed system under deregulated scenario. The delay margin results for constant time delay ($\mu = 0$) for different fractional orders ($\lambda = 0.1$ to 0.4 and 0.6 & 0.8) have been summarised.

6.2.2 | Poolco based transaction:-

Poolco-based operations, in which DISCOs have a contract with other GENCOs in the same area, involve all GENCOs equally. A load disturbance of 0.1 p.u (MW) is occurred in area-1. In this example study, time delays= τ_d 3.521 sec to 8.265sec are employed as a constant time delay ($\mu = 0$) for area-1, area-2 and area-3 respectively. Consider the following scenario, where $DISCO_1$, $DISCO_2$ have a power contract with other $GENCO_1$, $GENCO_2$ and $GENCO_3$ which is represented by a DPM

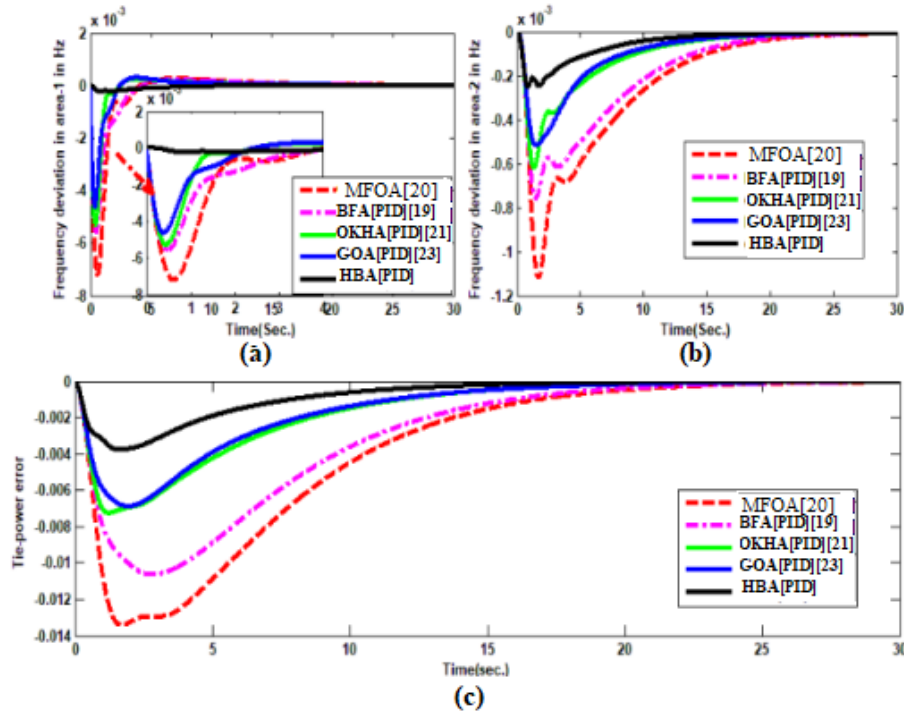


FIGURE 4 (a) Frequency deviation in area-1 in Hz $p.u.$ (b) Frequency deviation in area-2 in Hz $p.u$ (c) Tie-power error in Mw in $p.u$

matrix²⁴: -

$$DPM = \begin{bmatrix} 0.5 & 0.5 & 0 & 0 \\ 0.25 & 0.25 & 0 & 0 \\ 0.25 & 0.25 & 0 & 0 \\ 0 & 0 & 0 & 0 \\ 0 & 0 & 0 & 0 \\ 0 & 0 & 0 & 0 \end{bmatrix} \quad (45)$$

Total generation must match the load demand in steady-state conditions, which is given by:-

$$\begin{bmatrix} \Delta P_{g1ss} \\ \Delta P_{g2ss} \\ \Delta P_{g3ss} \\ \Delta P_{g4ss} \\ \Delta P_{g5ss} \\ \Delta P_{g6ss} \end{bmatrix} = \begin{bmatrix} 0.5 & 0.5 & 0 & 0 \\ 0.25 & 0.25 & 0 & 0 \\ 0.25 & 0.25 & 0 & 0 \\ 0 & 0 & 0 & 0 \\ 0 & 0 & 0 & 0 \\ 0 & 0 & 0 & 0 \end{bmatrix} \begin{bmatrix} 0.1 \\ 0.1 \\ 0.0 \\ 0.0 \end{bmatrix} \quad (46)$$

Simulations are conducted primarily for time constant time delay using a fractional order PI controller with fractional order (λ) ranging from 0 to 1. The empirical bode analysis approach is used to calculate the delay margin, as shown in Tables 3-6. In case of constant time delay ($\mu = 0.0$), the delay margin of τ_{dm} grows (from 3.521 sec. to 7.102 sec) with rising value of fractional order ($\lambda = 0.1$ to 0.4) for a set of K_p and K_I values within a particular range ($0.3 < K_p < 0.4$ & $0.4 < K_I < 0.6$). The stability range for a FOPI controller with fractional order $\lambda = 0.6$ for $\tau_d = 7.102$ sec. same as time varying delay $\tau_d = 8.265$ sec with fractional order $\lambda = 0.8$. So that, for $K_p > 0.4$ or $K_I > 0.6$, the system moves into an unstable zone for time varying delay $\tau_d = 8.265$ sec with fractional order $\lambda = 0.8$ and $\tau_d = 7.102$ sec. with fractional order $\lambda = 0.4$ of FOPI controller. System stability for HBA tuned P-I controller ($K_{I1} = 0.4166$; $K_{P1} = 0.3066$; $K_{I2} = 0.5541$; $K_{P2} = 0.3101$; $K_{I3} = 0.5641$; $K_{P3} = 0.3106$) with fraction order $\lambda = 0.8$, approaches a stable area, as shown in Figs. 6(a)-(b).

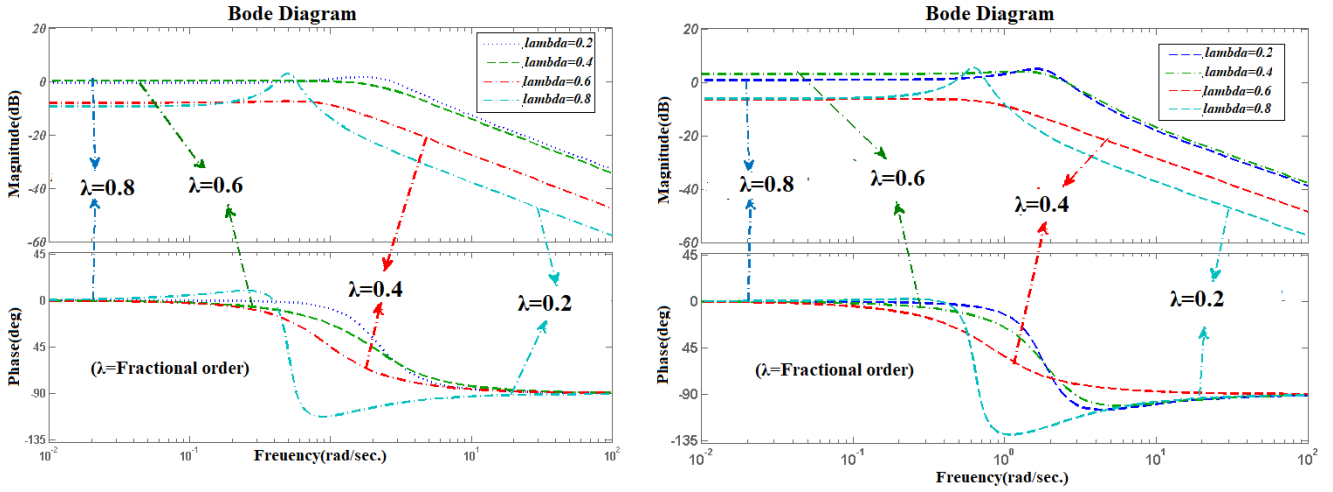


FIGURE 5 (a) Bode diagram when ($\mu = 0.0$) for constant time delay at $\tau_d=7.102$ sec. in unilateral case. (b) Bode diagram when ($\mu = 0$) for time delay at $\tau_d=7.234$ sec. in unilateral case.

TABLE 3 Stability analysis for $0.3 \leq K_p \leq 0.4$ & $0.4 \leq K_I \leq 0.6$ using gain margin (GM) and phase margin (PM) from bode plots for specified Time delay (τ_d)

Gain of K_p & K_I with fractional order (λ)	GM ($\mu = 0.0$) at ' $\tau_d = 7.102$ sec.'	PM ($\mu = 0.0$) at ' $\tau_d = 7.102$ sec.'	Delay margin (τ_{dm})	Stability
$\lambda = 0.2, K_p=0.3021:0.3789:0.3112, K_I=0.4603:0.5914:0.5861$	4.786dB	-1.086^0	6.542 sec.	No
$\lambda = 0.4, K_p=0.3692:0.3021:0.3214, K_I=0.4786:0.6012:0.5314$	7.56 dB	0^0	7.102 sec.	Marginally stable
$\lambda = 0.6, K_p=0.3066:0.4166:0.3101, K_I=0.5541:0.3106:0.5041$	1.925dB	∞	∞ sec.	yes
Gain of K_p & K_I with fractional order (λ)	GM ($\mu = 0.0$) at ' $\tau_d = 6.328$ sec.'	PM ($\mu = 0.0$) at ' $\tau_d = 6.328$ sec.'	Delay margin (τ_{dm})	Stability
$\lambda = 0.1, K_p=0.321:0.396:0.3061, K_I=0.573:0.516:0.5647$	1.184dB	-1.025^0	3.521 sec.	No
$\lambda = 0.3, K_p=0.3357:0.321:0.4021, K_I=0.5502:0.574:0.5106$	11.03dB	5.625^0	6.328 sec.	Marginally stable
$\lambda = 0.8, K_p=0.375:0.3127:0.3571, K_I=0.544:0.601:0.5974$	1.0856 dB	∞	8.265 Sec	Yes

For steady operation range of K_p & K_I are $0.3 \leq K_p \leq 0.4$ and $0.4 \leq K_I \leq 0.6$, where the value of fractional order of FOPI controller should be bigger than 0.4 ($\lambda \geq 0.4$) for constant time delay ($\mu = 0$) at $\tau_d = 7.234$ sec. As a result, the system lost its stability approach towards oscillation mode for $K_p > 0.4$ or $K_I > 0.6$ at $\tau_d = 7.234$ sec. On the other side, as fractional order decreases, the system becomes unstable ($\lambda = 0.4$ to 0.2), even if the range of K_p and K_I ($0.4 \leq K_I \leq 0.6$ & $0.3 \leq K_p \leq 0.4$) is maintained. A simulation-based delay margin further demonstrates that the suggested HBA tuned FOPI controller is capable of achieving system stability with specific range of fractional orders ($0.4 \leq \lambda \leq 0.8$). The dynamic responses for frequency deviation in area-1 & area-2 in the situation of constant time delay are presented in Fig. 6(c). The simulation results clearly show that as the value of λ decreases, the oscillations become more unstable, whereas as the fractional order (λ) increases, the oscillations slowly die out. For time delay ($\tau_d = 8.265$ sec.), dynamic response for HBA tuned FOPI with fractional order $\lambda = 0.8$ steady state (ST/ 4.19 sec. / Δf_1) is considerably faster than fractional order $\lambda = 0.4$ (ST/17.12 sec./ Δf_1). From the standpoint of stability, HBA-based FOPI with fractional order $\lambda = 0.8$ yields the lowest values of the ITSE, OS, US, and ST.

The simulation results serve in verifying the accuracy of the empirical bode analysis used to calculate the delay margin. FOPI controller lies in stable region for time varying delay as well as constant time delay with specific fractional order λ during the design of the LFC scheme under unilateral condition, which has been verified through dynamic responses of the time delayed hybrid system under unilateral condition.

6.2.3 | Bilateral Transaction:-

In the bilateral case, constant time delay $\tau_d = 3.014$ sec and $\tau_d = 4.325$ sec for λ are considered. For bilateral contract, power is transferred from the GENCO to the own DISNCO as well as other area DISCOs. A change in the DPM matrix in this scenario

TABLE 4 Delay margin for fractional order FOPI controller
 $\mu = 0$ (For constant time delay)^{42,43} fractional order $\lambda = 0.1$

K_p	Unilateral contract (K_I)						Bilateral Contract (K_I)					
	For $\tau_d = 3.521sec.$ $0.3 \leq K_p \leq 0.4$ & $0.4 \leq K_I \leq 0.6$						For $\tau_d = 2.245sec.$ $0.3 \leq K_p \leq 0.4$ & $0.4 \leq K_I \leq 0.6$					
0.1	18.69	16.55	12.05	5.624	3.921	1.625	3.854	4.201	4.869	2.935	2.899	3.675
0.2	11.95	10.02	7.965	3.875	3.118	1.496	3.447	4.268	3.512	2.754	1.985	2.489
0.3	10.16	8.056	7.112	3.886	3.112	2.076	3.021	3.954	2.887	2.335	1.357	4.367
0.4	6.562	4.021	3.521	3.021	2.567	1.456	3.124	2.964	2.245	2.004	1.33	3.925
0.5	4.865	4.345	3.662	2.632	2.016	1.425	1.665	1.565	1.242	1.056	0.995	1.589
0.6	3.596	3.945	2.867	3.112	2.079	1.895	1.112	1.668	2.019	1.662	2.435	3.167
0.7	2.567	2.231	1.892	1.652	1.106	0.765	1.557	1.356	1.662	2.009	1.361	2.461
0.8	1.210	2.142	1.667	1.251	1.324	0.462	0.541	1.092	1.117	0.625	1.092	1.312
0.9	0.657	1.351	1.452	1.001	0.967	0.456	0.974	1.221	1.621	0.462	1.012	1.217
1.0	0.524	0.746	0.532	0.447	0.608	0.346	0.445	0.562	0.947	0.436	1.025	1.401
1.1	0.376	0.228	0.314	0.537	0.258	0.462	1.021	0.312	1.006	0.537	0.628	1.229

K_p	Unilateral contract (K_I)						Bilateral Contract (K_I)					
	For $\tau_d = 4.032sec.$ $0.3 \leq K_p \leq 0.4$ & $0.4 \leq K_I \leq 0.6$						For $\tau_d = 2.776sec.$ $0.3 \leq K_p \leq 0.4$ & $0.4 \leq K_I \leq 0.6$					
	0.2	0.4	0.6	0.8	1.0	1.2	0.2	0.4	0.6	0.8	1.0	1.2
0.1	15.03	11.43	9.64	6.321	2.035	0.325	9.821	7.69	5.035	3.254	2.132	1.117
0.2	13.24	10.25	8.115	6.796	2.115	1.254	10.12	8.254	6.785	3.285	2.875	1.085
0.3	12.98	8.641	7.125	6.549	3.102	0.956	7.625	6.166	4.225	2.789	2.995	4.675
0.4	8.652	6.385	4.032	3.685	2.295	0.792	3.654	4.325	2.776	1.602	2.469	3.679
0.5	8.110	7.110	6.542	4.825	1.259	0.992	3.356	2.976	3.214	3.679	2.224	3.025
0.6	7.665	6.532	3.102	2.516	1.296	0.561	3.691	3.998	2.976	1.965	2.291	1.765
0.7	7.869	3.271	1.652	2.109	0.567	0.329	0.1576	1.254	2.302	3.021	2.163	1.219
0.9	6.894	3.102	1.851	0.867	0.325	0.112	0.916	1.096	2.954	2.110	1.657	2.957
1.0	5.789	1.129	0.649	0.320	0.109	0.096	1.127	2.254	1.897	2.214	1.627	2.961
1.1	1.425	0.697	0.527	0.339	0.246	0.194	0.762	1.165	1.562	1.602	1.658	2.118
1.2	0.557	0.395	0.302	0.114	0.259	0.112	1.112	2.621	2.102	1.579	1.221	2.187

can be stated as ²⁴:-

$$DPM = \begin{bmatrix} 0.1 & 0.2 & 0.5 & 0.3 \\ 0.2 & 0.1 & 0 & 0.1 \\ 0.0 & 0.1 & 0.3 & 0.2 \\ 0.3 & 0.2 & 0.1 & 0.1 \\ 0.2 & 0.3 & 0.0 & 0.1 \\ 0.2 & 0.1 & 0.1 & 0.2 \end{bmatrix} \quad (47)$$

The following values are created to meet demand and maintain the system's steady-state:—

$$\left. \begin{aligned} \Delta P_{g1ss} &= 0.11P.u.(Mw); \\ \Delta P_{g2ss} &= 0.03P.u.(Mw); \\ \Delta P_{g3ss} &= 0.06P.u.(Mw); \\ \Delta P_{g4ss} &= 0.07P.u.(Mw); \\ \Delta P_{g5ss} &= 0.06P.u.(Mw); \\ \Delta P_{g6ss} &= 0.06P.u.(Mw); \end{aligned} \right\} \quad (48)$$

The dynamic response depicts that fractional order $\lambda = 0.4$, the system evolves towards an unstable area when $K_p > 0.4$ and $K_I > 0.6$ for $\tau_d = 4.325sec.$ When the time delay τ_d is shorter than the delay margin ($\tau_{dm} < \tau_d$), the oscillations fade away and the system's response approaches a stable area, which can be achieved using the HBA technique. As demonstrated in Table 8, the gain value of a FOPI controller based on HBA is within the delay margin. As described in section 3.1, the delay margin is mostly estimated using empirical BODE analysis. The simulation results are first used to investigate the delay margin for a

TABLE 5 Delay margin for fractional order FOPI controller

$\mu = 0$ (For constant time delay) ^{42,43} fractional order $\lambda = 0.3$												
K_p	Unilateral contract (K_I)						Bilateral Contract (K_I)					
	For $\tau_d = 6.328\text{sec}$. $0.3 \leq K_p \leq 0.4$ & $0.4 \leq K_I \leq 0.6$						For $\tau_d = 3.014\text{sec}$. $0.05 \leq K_p \leq 0.3$ & $0.1 \leq K_I \leq 0.2$					
0.1	20.55	18.33	7.651	5.951	3.891	2.321	4.412	5.042	3.379	2.402	1.875	2.024
0.2	11.03	12.54	6.689	4.328	2.887	1.957	3.135	2.781	1.878	1.562	1.251	2.012
0.3	8.861	6.669	5.032	3.102	2.451	1.210	2.965	3.701	2.425	1.861	1.560	2.865
0.4	7.765	6.562	6.328	4.321	1.746	1.152	2.954	3.613	3.014	1.814	1.583	3.189
0.5	4.576	5.176	3.954	2.021	2.689	1.290	0.989	1.476	1.435	1.902	1.117	2.452
0.6	3.897	4.108	2.759	2.591	2.113	1.995	1.195	1.005	2.294	1.501	0.752	0.531
0.7	2.292	2.012	1.765	1.425	1.140	0.762	1.421	1.097	1.712	2.439	1.392	3.057
0.8	1.337	2.154	1.619	1.379	1.134	0.731	0.632	1.193	1.575	0.925	1.349	1.125
0.9	0.701	1.693	1.228	0.924	1.135	1.477	0.7254	1.098	1.299	0.719	1.125	1.369
1.0	0.577	0.919	0.717	0.795	0.601	0.389	0.652	1.025	1.569	1.229	0.987	1.125
1.1	0.695	0.762	0.479	0.964	0.351	0.7161	1.596	1.125	0.993	0.412	0.817	1.227
$\mu = 0.0$ ^{42,43} fractional order $\lambda = 0.4$												
K_p	Unilateral contract (K_I)						Bilateral Contract (K_I)					
	For $\tau_d = 7.102\text{sec}$. $0.3 \leq K_p \leq 0.4$ & $0.4 \leq K_I \leq 0.6$						For $\tau_d = 4.325\text{sec}$. $0.3 \leq K_p \leq 0.4$ & $0.4 \leq K_I \leq 0.6$					
	0.2	0.4	0.6	0.8	1.0	1.2	0.2	0.4	0.6	0.8	1	1.2
0.1	20.21	13.51	7.214	6.541	3.0285	0.785	9.842	7.698	5.785	3.894	3.185	2.441
0.2	19.54	14.25	9.584	7.895	2.854	1.334	9.798	8.195	5.445	3.025	2.051	3.195
0.3	20.54	10.29	8.065	7.968	1.462	0.115	7.956	5.036	3.016	3.025	2.112	2.956
0.4	20.65	8.325	7.102	4.912	1.952	0.234	5.165	4.225	4.325	2.521	2.028	3.235
0.5	21.03	8.432	6.102	3.895	1.229	0.109	3.295	4.069	3.194	3.526	2.445	3.012
0.6	20.02	6.105	3.025	2.052	1.102	0.292	2.002	3.896	3.399	3.112	2.092	2.145
0.7	17.89	3.563	2.353	1.869	0.659	0.259	2.405	2.559	3.755	4.119	1.895	3.757
0.8	10.02	2.672	1.652	0.812	0.702	0.235	1.775	1.572	2.095	2.685	1.775	3.025
0.9	5.726	1.115	0.8325	0.720	0.514	0.232	1.362	2.012	2.105	2.899	1.852	2.954
1.1	1.586	0.772	0.835	0.312	0.739	0.445	0.742	2.332	3.025	2.425	1.667	2.547
1.1	0.778	0.5471	0.5124	0.6951	0.3591	0.2421	1.227	2.521	2.901	2.039	1.001	2.135

constant time delay ($\mu = 0.0$) with a delay of $\tau_d = 4.325 \text{ sec}$. Fig. 7(a) depicts the system's response. The stability limit of the FOPI controller for time variable delay ($\tau_d = 4.325 \text{ sec}$) is $0.3 \leq K_p \leq 0.4$ & $0.4 \leq K_I \leq 0.6$ (K_p & K_I) for fractional order range ($0.4 \leq \lambda \leq 0.6$).

Time delay is evaluated as $\tau_d = 3.014 \text{ sec}$ for constant time delays ($\mu = 0$). The TD attack decreases the system's performance and pushes it towards an unstable zone, as seen in Figs. 7 (a-c). Similar conclusions may be drawn from those findings, which show that an HBA-based FOPI controller with fractional order $\lambda = 0.3$ is capable of achieving system stability within a delay margin. However, lowering the fractional order from $\lambda = 0.8$ to 0.3 renders the system slow and takes a long time to achieve steady state (ST/29.14s ec./ Δf_1). However, increasing the value of fractional order ($\lambda = 0.3$ to 0.8) at constant time delay ($\mu = 0$) can improve it efficiently (ST/9.87 sec./ Δf_1). As a result, the proposed coordinated HBA tuned FOPI controller with fractional order $\lambda = 0.8$ has better dynamic response and gives better overshoot, undershoot, and settling time, which can assist to a sufficient increase in stability and quickly restore the frequency and tie-line power to their steady state value. The HBA tuned FOPI with greater order of fraction delivers the best dynamic response and has better overshoot (OS), undershoot (US), and settling time (ST) (as seen in the dynamic responses).

6.2.4 | Contract violation

The results are checked in case of contract violation to authenticate the effectiveness of the proposed HBA algorithm in case of constant time delay of $\tau_d = 6.089 \text{ sec}$ & constant time delay of $\tau_d = 3.291 \text{ sec}$. Table 9 shows the optimum gain values of the K_p and K_I of FOPI controllers achieved by the suggested HBA algorithm for various fractional ($\lambda = 0.1$ to $0.4, 0.6$ & 0.8) orders. The FOPI controller gain values are also given with a delay margin ($0.05 \leq K_p \leq 0.4$ & $0.1 \leq K_I \leq 0.6$),

TABLE 6 Delay margin for fractional order FOPI controller

$\mu = 0$ (For constant time delay) ^{42,43} fractional order $\lambda = 0.6$												
K_P	Unilateral contract (K_I)						Bilateral Contract (K_I)					
	For $\tau_d = 7.234sec.$ $0.3 \leq K_P \leq 0.4$ & $0.4 \leq K_I \leq 0.6$						For $\tau_d = 4.112sec.$ $0.3 \leq K_P \leq 0.4$ & $0.4 \leq K_I \leq 0.6$					
0.1	30.225	21.025	17.85	12.24	7.845	6.621	4.425	4.105	3.102	2.785	2.102	2.522
0.2	15.03	13.02	11.054	7.895	6.425	3.775	2.471	1.987	3.657	1.442	1.014	2.957
0.3	12.34	8.964	9.163	4.752	3.254	1.476	3.95	4.302	4.112	2.103	1.897	3.147
0.4	6.725	7.258	7.234	4.067	1.897	1.251	3.478	2.897	3.255	1.987	1.425	3.752
0.5	5.761	4.325	3.965	2.462	2.229	1.658	1.289	0.896	1.987	1.625	1.235	2.785
0.6	4.789	3.987	3.125	2.995	2.257	1.992	1.025	0.954	2.654	1.972	1.065	0.765
0.7	2.189	1.892	1.567	1.665	1.140	0.967	1.314	1.005	1.254	2.957	1.659	3.992
0.8	2.567	2.068	1.954	1.462	1.203	0.941	0.786	1.335	1.776	1.292	1.465	1.214
0.9	0.981	1.975	1.524	1.321	1.213	1.577	0.925	1.945	1.542	0.967	1.456	1.251
1.0	0.964	0.867	0.627	0.430	0.612	0.967	0.183	1.235	1.569	1.798	0.887	1.035
1.1	0.767	0.625	0.514	0.320	0.102	0.9614	1.897	1.234	0.975	0.532	0.977	1.876

$\mu = 0.0$ (For constant time delay) ^{42,43} fractional order $\lambda = 0.8$												
K_P	Unilateral contract (K_I)						Bilateral Contract (K_I)					
	For $\tau_d = 8.265sec.$ $0.3 \leq K_P \leq 0.4$ & $0.4 \leq K_I \leq 0.6$						For $\tau_d = 4.025sec.$ $0.3 \leq K_P \leq 0.4$ & $0.4 \leq K_I \leq 0.6$					
	0.2	0.4	0.6	0.8	1.0	1.2	0.2	0.4	0.6	0.8	1.0	1.2
1.0	30.02	26.62	14.45	12.24	6.85	3.525	14.64	12.24	8.785	6.954	5.784	4.321
0.2	22.65	18.75	12.90	9.451	8.354	3.452	11.147	10.075	7.652	5.847	3.995	2.652
0.3	21.54	17.58	11.71	10.375	8.475	3.654	6.487	4.321	2.801	2.224	1.841	2.024
0.4	10.04	9.524	8.265	6.147	4.320	1.221	0.992	3.954	4.025	2.721	1.942	2.864
0.5	21.99	14.25	10.02	8.765	6.754	0.541	2.574	2.728	2.002	1.954	3.957	7.015
0.6	19.75	9.754	7.871	4.574	3.024	1.279	2.995	3.976	4.652	3.214	1.954	2.745
0.7	18.92	9.471	6.974	5.471	3.114	1.287	2.975	3.102	3.897	4.775	1.947	3.257
0.8	12.25	7.651	3.14	1.847	0.702	0.235	1.258	1.957	2.147	2.775	1.525	3.147
0.9	6.021	2.154	0.987	0.564	0.314	0.127	1.678	2.758	2.564	3.287	1.957	3.002
1.0	1.425	0.772	0.9325	0.757	0.8725	0.652	0.512	3.214	3.324	2.214	1.857	2.957
1.1	0.978	0.625	0.312	0.725	0.478	0.342	1.574	2.521	3.775	2.432	1.467	2.025

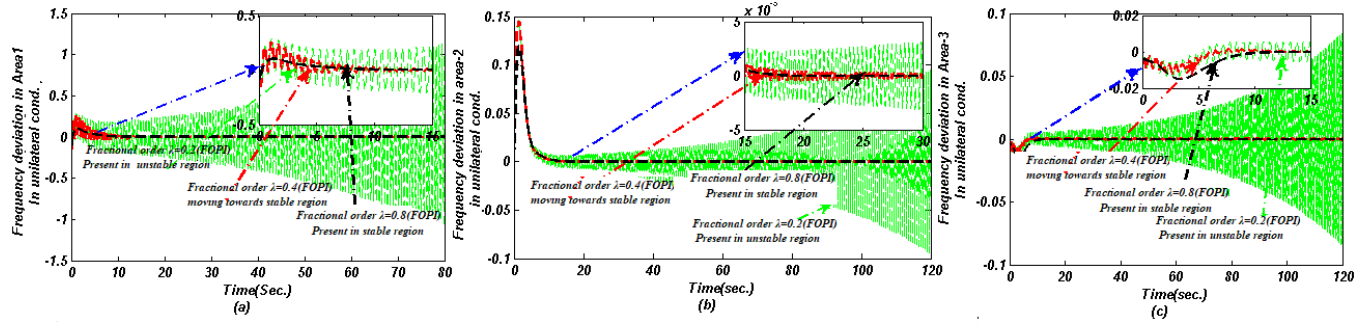
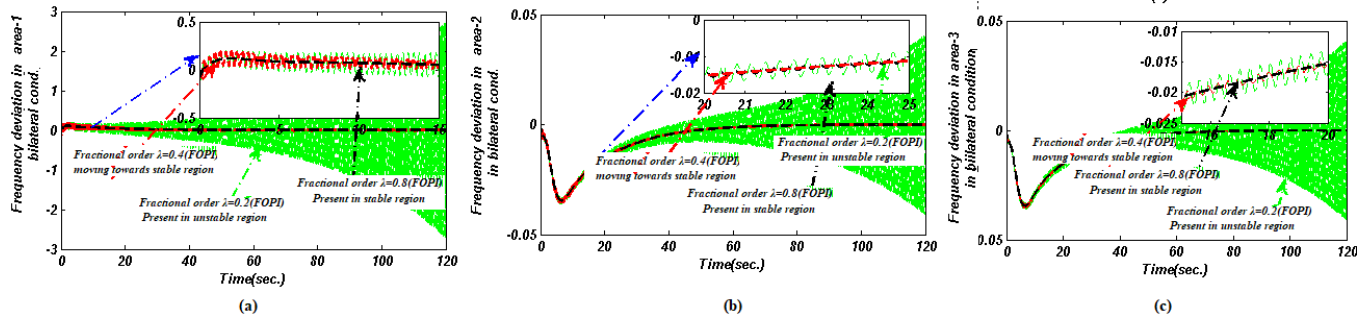
TABLE 7 Gain values of FOPI controllers for Thermal-solar-wind system (Test system-2)with DGS under deregulated environment in unilateral condition with time delays

Fractional Order	$0.3 \leq K_p \leq 0.4 & 0.4 \leq K_I \leq 0.6$ (table - 1&2&4)								Δf_1			Δf_2			Δf_3		
	K_{p1}	K_{I1}	K_{p2}	K_{I2}	K_{p3}	K_{I3}	$OBJ \times 10^{-2}$	OS	US	SS	OS	US	SS	OS	US	SS	OS
$\lambda = 0.2$	$\tau_d = 7.102'$ with $\mu = 0.0$								HBA Tuned FOPI controller with fractional order $\lambda = 0.2$ go towards unstable system								
$\lambda = 0.4$	$\tau_d = 7.102'$ with $\mu = 0.0$								0.263	-0.148	18.44	0.1457	-0.0002	35.12	0.0003	-0.129	14.48
$\lambda = 0.6$	$\tau_d = 7.102'$ with $\mu = 0.0$								0.9034	-0.09614	17.12	0.3148	-0.005641	10.24	0.00521	-0.0651	8.99
$\lambda = 0.8$	$\tau_d = 7.102'$ with $\mu = 0.0$								0.1034	-0.08831	4.19	0.1193	-0.0002491	8.12	0.000166	-0.00365	8.72
Fractional Order	$0.3 \leq K_p \leq 0.4 & 0.4 \leq K_I \leq 0.6$ (table - 1&2&4)								Δf_1			Δf_2			Δf_3		
	K_{p1}	K_{I1}	K_{p2}	K_{I2}	K_{p3}	K_{I3}	$OBJ \times 10^{-2}$	OS	US	SS	OS	US	SS	OS	US	SS	OS
$\lambda = 0.2$	$\tau_d = 6.328'$ with $\mu = 0.0$								HBA Tuned FOPI controller with fractional order $\lambda = 0.2$ go towards unstable system								
$\lambda = 0.4$	$\tau_d = 6.328'$ with $\mu = 0.0$								0.476	-0.236	31.24	0.1764	-0.02276	16.2	0.0004142	-0.0154	18.6
$\lambda = 0.6$	$\tau_d = 6.328'$ with $\mu = 0.0$								0.4512	-0.0165	5.97	0.674	-0.00447	8.63	0.00446	-0.0128	7.124
$\lambda = 0.8$	$\tau_d = 6.328'$ with $\mu = 0.0$								0.2239	-0.00912	11.24	0.01294	-0.001967	5.78	0.0000158	-0.00135	6.532

which is derived using empirical bode plot analysis. In a contract violation case, DISCO breaks the contract by demanding more electricity from GENCO than is specified in the contract. Extra amount of power 0.1 p.u (Mw) is demanded by DISCO, so that $\Delta P_{uc1} = 0.1$ p.u (Mw), $\Delta P_{uc2} = 0.0$; $\Delta P_{uc3} = 0.0$; $\Delta P_{uc4} = 0.0$. The rest of the scenarios are the same as they were in the bilateral transaction. Therefore, $\Delta P_{uc1} + \Delta P_{uc1,loc1} = \Delta P_{uc1,loc1} = 0.1 + 0.0 = 0.1$ p.u (Mw). and $\Delta P_{uc1,loc2} = \Delta P_{uc3} + \Delta P_{uc4} = 0.0$ p.u (Mw). In the event of a contract violation scenario, the ACE participation factor (apf) plays a critical part in violating the contract between

TABLE 8 Gain values of FOPI controllers for Thermal-solar-wind system (Test system-2)with DGS under deregulated environment in bilateral condition with time delays

Fractional Order	0.3 ≤ K _p ≤ 0.4 & 0.4 ≤ K _I ≤ 0.6 (table - 1&2&4)								Δf ₁		Δf ₂		Δf ₃			
	K _{p1}	K _{I1}	K _{p2}	K _{I2}	K _{p3}	K _{I3}	OBJ × 10 ⁻²	OS	US	SS	OS	US	SS	OS	US	SS
λ = 0.2	HBA Tuned FOPI controller with fractional order λ = 0.2 go towards unstable system															
τ _d = 4.325' with μ = 0.0	0.3712	0.5009	0.3624	0.4769	0.3974	0.567	1.447									
λ = 0.4	0.3559	0.5016	0.3926	0.5789	0.3007	0.5617	0.6054	0.01097	-0.003791	50.71	0.5612	-0.196	10.26	0.9.17	-0.657	30.28
λ = 0.6	0.3398	0.598	0.3547	0.5617	0.3097	0.4758	0.1421	0.2794	-0.1952	6.57	0.1192	-0.8132	7.12	0.3174	-0.574	14.34
λ = 0.8	0.3054	0.5007	0.3917	0.5465	0.3214	0.5052	0.0741	0.1174	-0.06734	3.83	0.0796	-0.0920	4.39	0.06731	-0.001176	8.42
Fractional Order	0.3 ≤ K _p ≤ 0.4 & 0.4 ≤ K _I ≤ 0.6 (table - 1&2&4)								Δf ₁		Δf ₂		Δf ₃			
	K _{p1}	K _{I1}	K _{p2}	K _{I2}	K _{p3}	K _{I3}	OBJ × 10 ⁻³	OS	US	SS	OS	US	SS	OS	US	SS
λ = 0.1	HBA Tuned FOPI controller with fractional order λ = 0.1 go towards unstable system															
τ _d = 3.014' with μ = 0.0	0.3010	0.5914	0.374	0.3947	0.313	0.5531	1.008									
λ = 0.3	0.3972	0.5701	0.3071	0.4348	0.3901	0.5147	0.7014	0.0129	-0.03457	49.4	0.074	-0.05271	36.4	0.005752	-0.0654	18.6
λ = 0.6	0.33952	0.4021	0.3965	0.4965	0.3925	0.3414	0.04312	0.005674	-0.01696	29.14	0.0167	-0.003398	18.63	0.00446	-0.0128	7.124
λ = 0.8	0.375	0.594	0.3127	0.601	0.3571	0.5974	0.00754	0.002239	-0.001054	9.87	0.00364	-0.01287	11.47	0.0000158	-0.00226	8.324

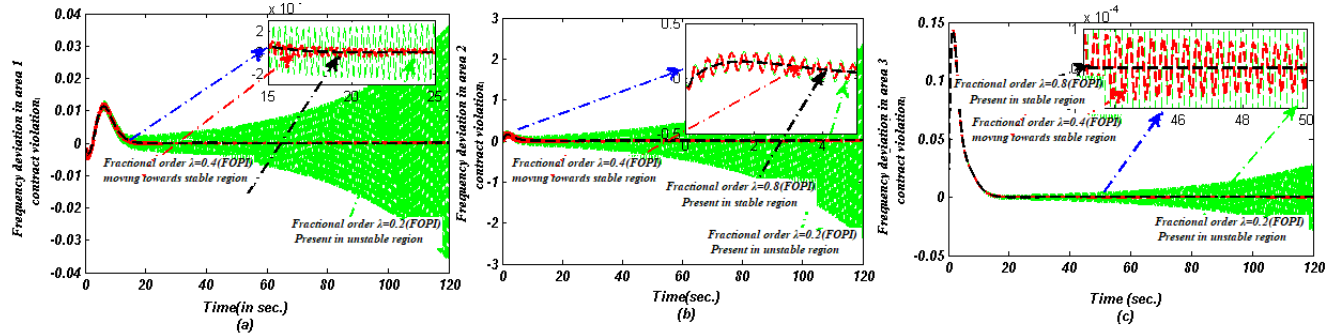
**FIGURE 6** (a)Area-1 frequency deviation for unilateral condition with 10% SLP type of load disturbance with time varying delay $\tau_d = 7.012 \text{ sec.}$ at a rate of $\mu = 0.0$. (b) Area-2 frequency deviation for unilateral scenario with 10 % SLP type of load with time varying delay $\tau_d = 7.012 \text{ sec.}$ at a rate $\mu = 0.0$. (c) Area-3 frequency deviation for for unilateral scenario with 10 % SLP type of load with constant time delay $\tau_d = 6.328 \text{ sec.}$ at a rate $\mu = 0.0$.**FIGURE 7** (a) Area-1 frequency deviation for Bilateral condition with a 10% SLP type of load with time varying delay $\tau_d = 4.325 \text{ sec.}$ at a rate $\mu = 0.0$. (b) Area-2 frequency deviation for Bilateral scenario 10% SLP type of load with constant time delay $\tau_d = 3.014 \text{ sec}$ at a rate of $\mu = 0.0$. (c) Area-3 frequency deviation for 10% SLP type of load with constant time delay w $\tau_d = 3.014 \text{ sec.}$ at rate of $\mu = 0.0$.

GENCOs and DISCOs.

$$\begin{bmatrix} \Delta P_{g1ss} \\ \Delta P_{g2ss} \\ \Delta P_{g3ss} \\ \Delta P_{g4ss} \end{bmatrix} = \begin{bmatrix} \text{cpf}_{11} & \text{cpf}_{12} & \text{cpf}_{13} & \text{cpf}_{14} \\ \text{cpf}_{21} & \text{cpf}_{22} & \text{cpf}_{23} & \text{cpf}_{24} \\ \text{cpf}_{31} & \text{cpf}_{32} & \text{cpf}_{33} & \text{cpf}_{34} \\ \text{cpf}_{41} & \text{cpf}_{42} & \text{cpf}_{43} & \text{cpf}_{44} \end{bmatrix} \begin{bmatrix} \Delta P_{L1} \\ \Delta P_{L2} \\ \Delta P_{L3} \\ \Delta P_{L4} \end{bmatrix} + \begin{bmatrix} \Delta P_{uc,Loc1} & 0 & 0 & 0 \\ 0 & \Delta P_{uc,Loc2} & 0 & 0 \\ 0 & 0 & \Delta P_{uc,Loc3} & 0 \\ 0 & 0 & 0 & \Delta P_{uc,Loc4} \end{bmatrix} \begin{bmatrix} \text{apf}_{11} \\ \text{apf}_{12} \\ \text{apf}_{13} \\ \text{apf}_{14} \end{bmatrix} \quad (49)$$

TABLE 9 Gain values of FOPI controllers for Thermal-solar-wind system (Test system-2) with DGS system under deregulated environment in contract violation condition with time delays

Fractional Order	$0.3 \leq K_p \leq 0.4 \& 0.4 \leq K_I \leq 0.6$ (table - 1&2&4)										Δf_1				Δf_2				Δf_3			
	K_{p1}	K_{I1}	K_{p2}	K_{I2}	K_{p3}	K_{I3}	$OBJ \times 10^{-2}$	OS	US	SS	OS	US	SS	OS	US	SS	OS	US	SS			
$\lambda = 0.2$	HBA Tuned FOPI controller with fractional order $\lambda = 0.2$ go towards unstable system																					
$\tau_d = 6.089'$ with $\mu = 0.5$	0.3671	0.4342	0.3012	0.5647	0.3301	0.5647	1.547															
$\lambda = 0.4$	HBA Tuned FOPI controller with fractional order $\lambda = 0.2$ go towards unstable system																					
$\tau_d = 6.089'$ with $\mu = 0.5$	0.3649	0.5012	0.3352	0.5741	0.3901	0.5019	0.8914	0.01097	-0.003791	50.71	0.6471	-0.05571	19.14	0.0127	-0.4758	34.12						
$\lambda = 0.6$	HBA Tuned FOPI controller with fractional order $\lambda = 0.2$ go towards unstable system																					
$\tau_d = 6.089'$ with $\mu = 0.5$	0.3924	0.4721	0.3772	0.5271	0.3102	0.5214	0.1401	0.00894	-0.002604	33.65	0.012945	-0.01014	12.24	0.00921	-0.00685	9.12						
$\lambda = 0.8$	HBA Tuned FOPI controller with fractional order $\lambda = 0.2$ go towards unstable system																					
$\tau_d = 6.089'$ with $\mu = 0.5$	0.3961	0.4108	0.3374	0.5814	0.3397	0.5712	0.0941	0.00167	-0.000765	12.08	0.0001987	-0.002954	5.97	0.0007625	-0.001192	6.94						
Fractional Order	$0.3 \leq K_p \leq 0.4 \& 0.4 \leq K_I \leq 0.6$ (table - 1&2&4)										Δf_1				Δf_2				Δf_3			
	K_{p1}	K_{I1}	K_{p2}	K_{I2}	K_{p3}	K_{I3}	$OBJ \times 10^{-2}$	OS	US	SS	OS	US	SS	OS	US	SS	OS	US	SS			
$\lambda = 0.1$	HBA Tuned FOPI controller with fractional order $\lambda = 0.1$ go towards unstable system																					
$\tau_d = 3.291'$ with $\mu = 0.0$	0.3094	0.5391	0.3602	0.5422	0.3658	0.5712	1.847															
$\lambda = 0.3$	HBA Tuned FOPI controller with fractional order $\lambda = 0.1$ go towards unstable system																					
$\tau_d = 3.291'$ with $\mu = 0.0$	0.3127	0.5464	0.3901	0.5667	0.3201	0.4967	0.0567	0.462	-0.03341	39.25	0.2315	-0.007499	20.12	0.1411	0	18.02						
$\lambda = 0.6$	HBA Tuned FOPI controller with fractional order $\lambda = 0.1$ go towards unstable system																					
$\tau_d = 3.291'$ with $\mu = 0.0$	0.396	0.5654	0.3142	0.5254	0.3647	0.5247	0.00147	0.001147	-0.0014	9.54	0.1942	-0.003267	14.22	0.09211	0	10.22						
$\lambda = 0.8$	HBA Tuned FOPI controller with fractional order $\lambda = 0.1$ go towards unstable system																					
$\tau_d = 3.291'$ with $\mu = 0.0$	0.3891	0.5022	0.3451	0.5714	0.3522	0.5214	0.001191	0.00214	-0.000142	6.24	0.1046	-0.000921	5.64	0.009164	0	4.67						

**FIGURE 8** (a) Area-1 frequency deviation for contract violation with SLP type load and 10% load disturbance with time varying delay $\tau_d = 6.089$ sec. at a rate $\mu = 0.0$. (b) Area-2 frequency deviation for contract violation case with SLP type of load and 10% load disturbance with constant time delay $\tau_d = 3.291$ sec at a rate of $\mu = 0.0$. (c) Frequency deviation of area-3 with constant time delay $\tau_d = 3.291$ sec. at a rate $\mu = 0.0$ at 10% load disturbance.**TABLE 10** Gain values of FOPI controller to (Test system 2) Hybrid thermal-wind-solar system With DGS constant time delays $\tau_d = 7.365$ sec and RLP type of load for ± 0.02 MW ($p.u.$).

$0.3 \leq K_p \leq 0.4 \& 0.4 \leq K_I \leq 0.6$	Optimized Parameter	Unilateral Contract				Bilateral Contract				Contract violation			
		FOPI ($\lambda = 0.2$)	FOPI ($\lambda = 0.4$)	FOPI ($\lambda = 0.8$)	FOPI ($\lambda = 0.2$)	FOPI ($\lambda = 0.4$)	FOPI ($\lambda = 0.8$)	FOPI ($\lambda = 0.2$)	FOPI ($\lambda = 0.4$)	FOPI ($\lambda = 0.8$)	FOPI ($\lambda = 0.2$)	FOPI ($\lambda = 0.4$)	FOPI ($\lambda = 0.8$)
P-I Controller with Fractional order 0.2, 0.4 & 0.8 &	K_{p1}	0.3036	0.354	0.3364	0.3017	0.3924	0.3195	0.3001	0.3109	0.3794			
	K_{I1}	0.571	0.5014	0.5892	0.5952	0.5010	0.5431	0.5974	0.5197	0.5661			
	K_{p2}	0.3296	0.3964	0.3345	0.3016	0.3891	0.3457	0.3914	0.3107	0.3761			
	K_{I2}	0.5012	0.5361	0.5714	0.5013	0.5512	0.5014	0.5991	0.5221	0.5691			
	K_{p3}	0.3120	0.3941	0.3241	0.3901	0.3410	0.3324	0.3741	0.3011	0.3951			
	K_{I3}	0.5941	0.5601	0.5901	0.5001	0.5447	0.5131	0.5201	0.5901	0.5461			
OBJ		1.231	0.621	0.1754	0.0674	0.0221	0.00754	0.002513	0.000954	0.000124			

As a result, area-1 demands surplus un-contract power, which is automatically compensated by $GENCO_2$, & $GENCO_3$ of area-2 and area-3. Therefore,

$$\left. \begin{aligned} \Delta P_{g_{1ss}} &= 0.18 p.u. (Mw); \\ \Delta P_{g_{2ss}} &= 0.1155 p.u. (Mw); \\ \Delta P_{g_{3ss}} &= 0.085 p.u. (Mw); \\ \Delta P_{g_{4ss}} &= 0.16 p.u. (Mw); \\ \Delta P_{g_{5ss}} &= 0.16 p.u. (Mw); \\ \Delta P_{g_{6ss}} &= 0.16 p.u. (Mw); \end{aligned} \right\} \quad (50)$$

Table 9 and Fig. 8 compare the performance of the FOPI controller with various fractional orders ($\lambda = 0.1, 0.4, 0.6$ & 0.8) by recording the dynamic responses of the multi-source hybrid system in the form of OS, US, and ST, as well as the objective function. The results show that the suggested HBA-based FOPI with fractional order $\lambda = 0.8$ is responsible for the greatest solution quality for K_p, K_I ($0.3 \leq K_p \leq 0.4$ & $0.4 \leq K_I \leq 0.6$) for time delays $\tau_d = 6.089$ sec. and $\tau_d = 3.291$ sec for the proposed AGC system.

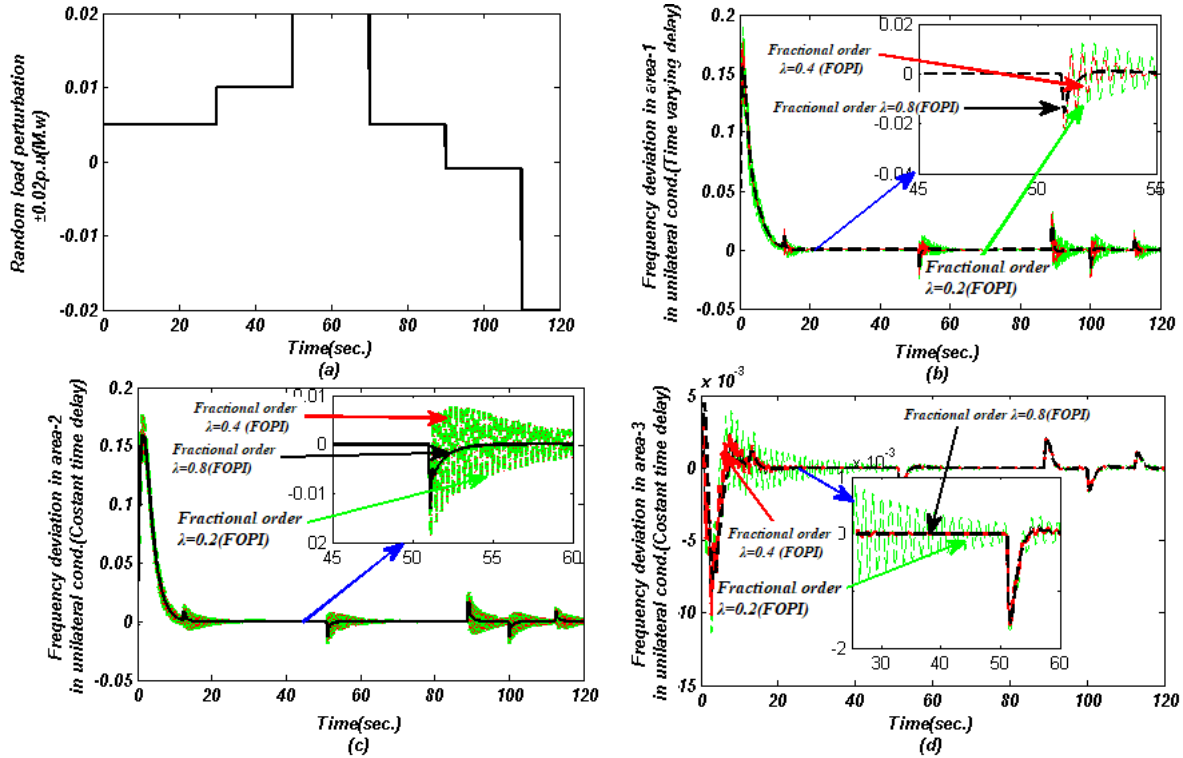


FIGURE 9 (a) Using a load of $\pm 0.02 p.u.$, random load perturbation was performed (Mw)(b) For a $\pm 0.02 (p.u)$ RLP type of load, frequency variation in area-1 in Hz for unilateral condition with time varying ($\tau_d = 7.365 sec.$) ($\mu = 0.0$) delay.(c) For a $\pm 0.02 (p.u)$ RLP type of load, frequency variation in area-2 in Hz for unilateral condition with time varying ($\tau_d = 7.365 sec.$) ($\mu = 0.0$) delay.(d) For a $\pm 0.02 (p.u)$ RLP type of load, frequency variation in area-3 in Hz for unilateral condition with constant time ($\tau_d = 5.127 sec.$) ($\mu = 0.0$) delay.

7 | ROBUSTNESS ANALYSIS OF THE PROPOSED METHOD

To test the robustness of the FOPI controller, a random load perturbation (RLP) is applied to area-1 of the supplied solar-wind-thermal system using the proposed HBA algorithm with different fractional orders (λ). The RLP load type value varies by $\pm 0.02 p.u$ (Mw).

A random step load change is applied in area-1 with a time delay $\tau_d = 7.365 sec$ to judge the robustness of the proposed HBA based FOPI controller under specified time delays. Fig. 9(a) depicts the RLP (random type of load) pattern applied to the suggested hybrid system. Under the deregulated scenario, the gain value of different parameters of the FOPI controller (within delay margin) is optimized simultaneously in three separate cases. The comparison results are shown in Table 10. As demonstrated in Fig. 9, the peak magnitude of frequency and tie-power oscillations with HBA based FOPI with fractional order ($\lambda = 0.8$) is quickly attenuated under RLP type of load, proving the robustness of HBA based FOPI controller.

8 | CONCLUSION

This article focuses on optimal delay tuning to overcome the communication delay problem during synchronisation of non-conventional (wind-solar) power plants with conventional energy plants in order to reduce dependency on traditional resources and bring renewable energy resources into the mainstream of the power generating sector (thermal plants). To assess the performance of the proposed HBA algorithm, initially, a two-area thermal system is studied, and a comparison is performed between HBA, OKHA, GOA, BFA, and MFOA. The HBA algorithm excels the GOA, OKHA, BFA and MFOA algorithms in terms of dynamic response. Furthermore, by considering time delays with a specified range of fractional order (λ) in the LFC

control loop, a delay dependent stability criterion is proposed to find the delay margin for fractional order proportional-integral controller (FOPI). It has been clearly analyzed how delay margin considerably fluctuates with different values of fractional order (λ) of FOPI controller for a certain range of delay. It has been observed that as the value of fractional order (λ) rises, the delay margin (τ_{dm}) increases in a renewable-based three-area hybrid system with distributed generation in a deregulated environment. Finally, it can be seen that a hybridised (Hybrid system with distributed generation) system has greater performance, since it can meet specific power requirements and minimize system oscillation totally.

The simulations' major conclusion can be described as follows:

- The delay margin of the FOPI controller is determined using empirical bode analysis (EBA), which may be used in design the controller for the aforesaid linearized time delayed system and verifying it using their dynamic performance in three different instances.
- Using the HBA method, all control parameters of the FOPI controller in area-1, area-2, and area-3 are stable within the permissible delay margin. Afterward, an experiment is run with a range of fractional order (λ from 0.2 to 0.8) for a FOPI controller with set of K_p and K_I values maintained within given delay margin. Investigation shows that frequency response and tie-line power fluctuations are strongly affected by the controller for a given time delay. Within a specified Control parameter set (K_p & K_I), fractional order (λ) may enhance delay margin (τ_{dm}).
- Use the RLP type of load to test the FOPI controller's resilience performance for the provided system.
- The findings show how the proposed controlling technique can make the hybrid system optimally stable over a wide range of delays.

The following research initiatives could be expanded in the future:

- Application of the suggested technique to AGC time delay systems with multiple areas (more than three).
- In case of random nature time delay in a multi-area system, structured singular value (SSV) and Shurcohn (Hemetic matrix creation) may determine MADB and provide a thorough stability study.
- (iii)The proposed method can be used to test the stability of a time delay system with advanced controllers (such as TID, two-degree-of-freedom (2DOF)-PID, 3DOF-PID, fractional-order-PID, cascade PI-PID, tilt-integral-derivative (TID), and cascade-TID (CC-TID)) that are designed to handle constant and time-varying delays.

Appendix A.(Renewable three-area hybrid system)

$B_1, B_2 = 0.425 p.u MW / Hz$; $R_1, R_2 = 2.4 Hz / pu$; $T_{G1} = 0.08s$; $T_{T1} = 0.3s$; $T_{r1} = 10s$; $K_{r1} = 0.3s$; $K_{P1} = 120 Hz / pu MW$; $K_{P2} = 120 Hz / pu MW$; $T_{P1} = T_{P2} = 20s$; $P_{tie12} = 200 MW$; $a_{12} = -1$, $X_G = 0.6s$; $Y_G = 1.1s$; $K_{T1} = K_{T2} = 0.6$; $T_{RH} = 41.6 s$, $T_R = 5 s$; $T_{GH} = 0.51 s$, $T_W = 1 s$, $K_{H1} = K_{H2} = 0.3$, $C_g = 1$; $b_g = 0.049s$; $T_F = 0.239s$; $T_{CR} = 0.01s$; $T_{CD} = 0.2s$; $RLP = \pm 0.02 p.u(Mw)$

Appendix B.(Value of solar-wind & distributed generation parameter)

$K_{IB} = 0.03$; $T_{IB} = 26$; $T_{RB} = 69$; $T_D = 0.1$; $K_1 = 0.85$; $K_2 = 1.25$; $K_3 = 0.92$; $C_B = 200$; $K_{WTG} = 0.3$; $T_{WTG} = 1.4$; $K_{AE} = 0.02$; $T_{AE} = 0.5$; $K_{FC} = 0.01$; $T_{FC} = 3$; $K_{DEG} = 0.03$; $T_{DEG} = 23$; $K_{BESS} = -0.003$; $T_{BESS} = 0.1$; $a = 900$; $b = -18$; $d = 50$; $K_{WT1} = 1.25$; $K_{WT2} = 1.10$; $T_{TP,WT1} = 0.3$; $T_{TP,WT2} = 0.65$; $K_r = 10$; $T_r = 0.5$; $K_{PS} = 120$; $T_{PS} = 20$; $\beta = 0.9$

References

1. Saha A, Saikia LC. Renewable energy source-based multiarea AGC system with integration of EV utilizing cascade controller considering time delay. *International Transactions on Electrical Energy Systems* 2019; 29(1): e2646.
2. Zhao X, He J, Fu B, He L, Xu G. A System Compensation Based Model Predictive AGC Method for Multiarea Interconnected Power Systems with High Penetration of PV System and Random Time Delay between Different Areas. *Mathematical Problems in Engineering* 2018; 2018.
3. Islam S, El Saddik A, Sunda-Meya A. Robust load frequency control for smart power grid over open distributed communication network with uncertainty. In: IEEE; 2019: 4341–4346.
4. Yan C, Fu L, Zhang J, Wang J. A comprehensive survey on UAV communication channel modeling. *IEEE Access* 2019; 7: 107769–107792.

5. Sharma D, Mishra S. Impacts of system non-linearities on communication delay margin for power systems having open channel communication based automatic generation control. In: IEEE. ; 2018: 1–5.
6. Ghany HA, Ahmad ES, Elgebaly AE. A Reliable Loss of Excitation Protection Technique based on EPFA for Synchronous Generators. *IEEE Transactions on Power Delivery* 2021.
7. Pokhrel SR, Kumar N, Walid A. Towards Ultra Reliable Low Latency Multipath TCP for Connected Autonomous Vehicles. *IEEE Transactions on Vehicular Technology* 2021; 70(8): 8175–8185.
8. Biswas S, Roy PK, Chatterjee K. Development of MADB of P-I controller using LMI technique in a renewable energy based AGC system and study its application in a deregulated environment including energy storage device. *Optimal Control Applications and Methods* 2021.
9. Suzuki M. Interpretation of the Schur-Cohn test in terms of canonical systems. *arXiv preprint arXiv:2106.04061* 2021.
10. Ebenbauer C, Allgower F. Stability analysis for time-delay systems using rekasius's substitution and sum of squares. In: IEEE. ; 2006: 5376–5381.
11. Huang B, Jiang S, Song Z, Tao R. Solving Tall Dense SDPs in the Current Matrix Multiplication Time. *arXiv preprint arXiv:2101.08208* 2021.
12. Chen L, Zhou T, Xu Z, Zhang T. Delay Margin Computation and Controller Design of Time-delayed AGC System Based on Root Locus Analysis. In: . 252. *EDP Sciences.* ; 2021: 01022.
13. Chakraborty S, Ghosh S, Naskar AK. All-PD control of pure integrating plus time-delay processes with gain and phase-margin specifications. *ISA transactions* 2017; 68: 203–211.
14. Ramírez A, Breda D, Sipahi R. A scalable approach to compute delay margin of a class of neutral-type time delay systems. *SIAM Journal on Control and Optimization* 2021; 59(2): 805–824.
15. Xiong L, Li H, Wang J. LMI based robust load frequency control for time delayed power system via delay margin estimation. *International Journal of Electrical Power & Energy Systems* 2018; 100: 91–103.
16. Babu NR, Bhagat SK, Saikia LC, Chiranjeevi T. Application of hybrid crow-search with particle swarm optimization algorithm in AGC studies of multi-area systems. *Journal of Discrete Mathematical Sciences and Cryptography* 2020; 23(2): 429–439.
17. Zhang F, Hu X, Langari R, Wang L, Cui Y, Pang H. Adaptive energy management in automated hybrid electric vehicles with flexible torque request. *Energy* 2021; 214: 118873.
18. Elsisi M, Soliman M, Aboelela M, Mansour W. GSA-based design of dual proportional integral load frequency controllers for nonlinear hydrothermal power system. *International Journal of Electrical, Computer, Energetic, Electronic and Communication Engineering* 2015; 9(8): 928–934.
19. Shouran M, Anayi F, Packianather M, Habil M. Load Frequency Control Based on the Bees Algorithm for the Great Britain Power System. *Designs* 2021; 5(3): 50.
20. Hakimuddin N, Nasiruddin I, Bhatti TS. Generation-based automatic generation control with multisources power system using bacterial foraging algorithm. *Engineering Reports* 2020; 2(8): e12191.
21. Mohanty B. Performance analysis of moth flame optimization algorithm for AGC system. *International Journal of Modelling and Simulation* 2019; 39(2): 73–87.
22. Goswami L, Biswas S, Dutta S, Roy PK. Load frequency control of multi area power system with de-regulation using OKHA. In: IEEE. ; 2017: 507–512.
23. Elsisi M, Bazmohammadi N, Guerrero JM, Ebrahim MA. Energy management of controllable loads in multi-area power systems with wind power penetration based on new supervisor fuzzy nonlinear sliding mode control. *Energy* 2021; 221: 119867.
24. Biswas S, Roy PK, Chatterjee K. FACTS-based 3DOF-PID Controller for LFC of Renewable Power System Under Deregulation Using GOA. *IETE Journal of Research* 2021: 1–14.
25. Hashim FA, Houssein EH, Hussain K, Mabrouk MS, Al-Atabany W. Honey badger algorithm: new metaheuristic algorithm for solving optimization problems. *Mathematics and Computers in Simulation* 2022; 192: 84–110.
26. Pradhan C, Gjengedal T. Adaptive Jaya Algorithm for Optimized PI-PD Cascade Controller of Load Frequency Control in Interconnected Two-Area Power System. In: IEEE. ; 2020: 181–186.
27. Daraz A, Malik SA, Waseem A, et al. Automatic Generation Control of Multi-Source Interconnected Power System Using FOI-TD Controller. *Energies* 2021; 14(18): 5867.
28. Ram Babu N, Chandra Saikia L. Automatic generation control of a solar thermal and dish-stirling solar thermal system integrated multi-area system incorporating accurate HVDC link model using crow search algorithm optimised FOPI Minus FODF controller. *IET Renewable Power Generation* 2019; 13(12): 2221–2231.
29. Dei G, Sahoo S, Sahu BK. Performance analysis of ALO tuned FOPID controller for AGC of a three area power system. In: IEEE. ; 2018: 3116–3120.
30. Arya Y. A novel CFFOPI-FOPID controller for AGC performance enhancement of single and multi-area electric power systems. *ISA transactions* 2020; 100: 126–135.
31. Debbarma S, Saikia LC, Sinha N. Automatic generation control using two degree of freedom fractional order PID controller. *International Journal of Electrical Power & Energy Systems* 2014; 58: 120–129.
32. Nayak JR, Shaw B, Sahu BK. Implementation of hybrid SSA–SA based three-degree-of-freedom fractional-order PID controller for AGC of a two-area power system integrated with small hydro plants. *IET Generation, Transmission & Distribution* 2020; 14(13): 2430–2440.
33. Biswas S, Kumar Roy P, Chatterjee K. Renewable Energy-Based Multi-source System Under Deregulated Environment Using COKHA Algorithm. *IETE Journal of Research* 2021: 1–19.

34. Cokmez E, Atiç S, Peker F, Kaya I. Fractional-order PI controller design for integrating processes based on gain and phase margin specifications. *IFAC-PapersOnLine* 2018; 51(4): 751–756.
35. Oshnoei S, Oshnoei A, Mosallanejad A, Haghjoo F. Contribution of GCSC to regulate the frequency in multi-area power systems considering time delays: A new control outline based on fractional order controllers. *International Journal of Electrical Power & Energy Systems* 2020; 123: 106197.
36. Ojaghi P, Rahmani M. LMI-based robust predictive load frequency control for power systems with communication delays. *IEEE Transactions on Power Systems* 2017; 32(5): 4091–4100.
37. Sharma D, Mishra S, Firdaus A. Multi objective gain tuning approach for time delayed automatic generation control. In: *IEEE*. ; 2017: 2896–2900.
38. Patel NC, Sahu BK, Debnath MK. Automatic generation control analysis of power system with nonlinearities and electric vehicle aggregators with time-varying delay implementing a novel control strategy. *Turkish Journal of Electrical Engineering & Computer Sciences* 2019; 27(4): 3040–3054.
39. Mohapatra G, Debnath MK, Mohapatra KK. IMO-based novel adaptive dual-mode controller design for AGC investigation in different types of systems. *Cogent Engineering* 2020; 7(1): 1711675.
40. Guha D, Roy PK, Banerjee S. Performance evolution of different controllers for frequency regulation of a hybrid energy power system employing chaotic crow search algorithm. *ISA transactions* 2021.
41. Elkawafi S, Khalil A, Elgaiyar AI, Wang J. Delay-dependent stability of LFC in Microgrid with varying time delays. In: *IEEE*. ; 2016: 354–359.
42. Jiang L, Yao W, Wu Q, Wen J, Cheng S. Delay-dependent stability for load frequency control with constant and time-varying delays. *IEEE Transactions on Power systems* 2011; 27(2): 932–941.
43. Farnam A, Efsanjani RM. Improved linear matrix inequality approach to stability analysis of linear systems with interval time-varying delays. *Journal of Computational and Applied Mathematics* 2016; 294: 49–56.

